JCI The Journal of Clinical Investigation

Elevated NR2F1 underlies the persistence of invasive disease after treatment of BRAF-mutant melanoma

Manoela Tiago, … , Julio A. Aguirre-Ghiso, Andrew E. Aplin

J Clin Invest. 2025. https://doi.org/10.1172/JCI178446.

Research In-Press Preview Oncology

Graphical abstract

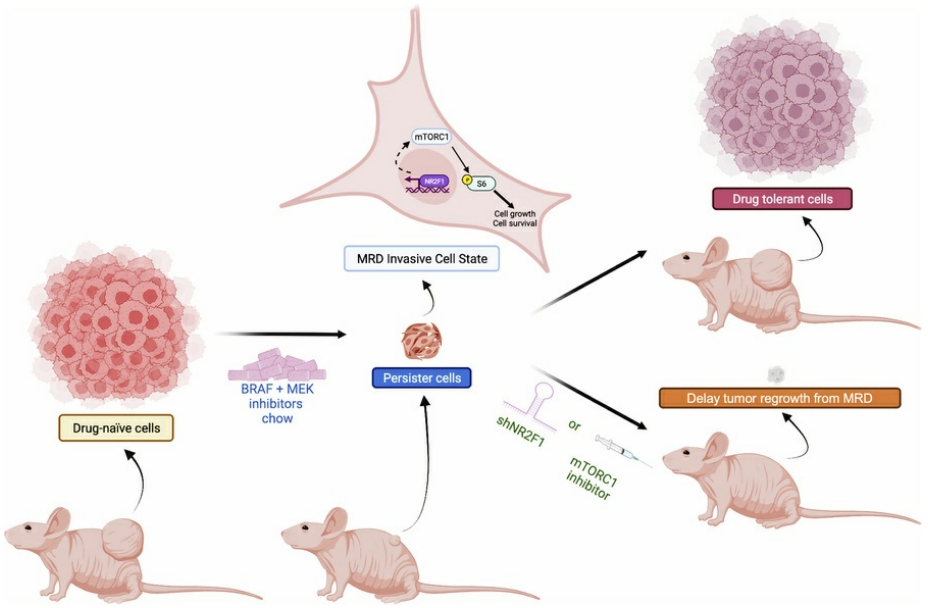

Elevated NR2F1 underlies the persistence of invasive disease after treatment of BRAF-mutant melanoma

Manoela Tiago[1], Timothy J. Purwin[1], Casey D. Stefanski[1], Renaira Oliveira da Silva[1, 2], Mitchell E. Fane[3], Yash Chhabra[3], Jelan I. Haj[1], Jessica L. F. Teh[1], Rama Kadamb[4], Weijia Cai[1,5], Sheera Rosenbaum[1], Vivian Chua[1], Nir Hacohen[6, 7, 8], Michael A. Davies[9], Jessie Villanueva[10], Inna Chervoneva[11,12], Ashani T. Weeraratna[13], Dan A. Erkes[1,12], Claudia Capparelli[12,14], Julio A. Aguirre-Ghiso[4], and Andrew E. Aplin[1,12]*

[1]Department of Pharmacology, Physiology, and Cancer Biology, Thomas Jefferson University, Philadelphia, PA. [2]Department of Clinical Chemistry and Toxicology, University of São Paulo, São Paulo, Brazil. [3]Department of Cancer Signaling and Microenvironment, Fox Chase Cancer Center, Temple Health, Philadelphia, PA. [4]Department of Cell Biology, Cancer Dormancy, and Tumor Microenvironment Institute, Gruss Lipper Biophotonics Center, Bronx, NY. [5]Department of Medical Microbiology, Immunology, and Cell Biology at SIU Medicine, Springfield, IL. [6]Broad Institute of MIT and Harvard, Cambridge, MA. [7]Department of Medicine, Center for Cancer Research, Massachusetts General Hospital, Boston, MA. [8]Department of Medicine, Harvard Medical School, Boston, MA. [9]Department of Melanoma Medical Oncology, The University of Texas MD Anderson Cancer Center, Houston, TX. [10]Molecular and Cellular Oncogenesis Program and Melanoma Research Center, The Wistar Institute, Philadelphia, PA. [11]Division of Biostatistics, Department of Pharmacology and Experimental Therapeutics, Thomas Jefferson University, Philadelphia, PA. [12]Sidney Kimmel Comprehensive Cancer Center, Thomas Jefferson University, Philadelphia, PA. [13]Department of Biochemistry and Molecular Biology, Johns Hopkins Bloomberg School of Public Health and Department of Oncology, Sidney Kimmel Comprehensive Cancer Center, Baltimore, MD. [14]Department of Medical Oncology, Thomas Jefferson University, Philadelphia, PA.

***Corresponding author**: Andrew E. Aplin, Department of Pharmacology, Physiology, and Cancer Biology, Sidney Kimmel Comprehensive Cancer Center, Thomas Jefferson University, 233 South 10th Street, Philadelphia, PA 19107. Tel: +1 (215) 503-7296. Fax: +1 (215) 923-9248; e-mail: Andrew.Aplin@jefferson.edu.

Running title: Residual disease in BRAF mutant melanoma.

Keywords: BRAF and MEK inhibitors; melanoma; drug-tolerant cells; residual disease; NR2F1.

Conflict of interest: A. E. Aplin has ownership interest in patent number 9880150. J. A. Aguirre-Ghiso is a scientific co-founder, scientific advisory board member, and equity owner in HiberCell and receives financial compensation as a consultant for HiberCell, a Mount Sinai spin-off company focused on the research and development of therapeutics that prevent or delay the recurrence of cancer. M. A. Davies has been a consultant to Roche/Genentech, Array, Pfizer, Novartis, BMS, GSK, Sanofi-Aventis, Vaccinex, Apexigen, Eisai, Iovance, Merck, and ABM Therapeutics; and he has been the PI of research grants to MD Anderson by AstraZeneca, Roche/Genentech, GSK, Sanofi-Aventis, Merck, Myriad, Oncothyreon, Pfizer, ABM Therapeutics, and LEAD Pharma. A. T. Weeraratna is on the board of ReGAIN therapeutics, unrelated to this work. D.A. Erkes has ownership interest in patent number US20200164054A1, unrelated to this work. Other authors have declared that no conflict of interest exists.

Financial support: This work is supported by grants from National Institutes of Health (NIH)/National Cancer Institute (1), R01 CA253977, R01 CA182635, and project 4 of P01 CA114046 to A. E. Aplin and J. Villanueva; and Department of Defense (HT9425-23-MRP-MASA-ME230214) and the W.W. Smith Charitable Trust Award to C. Capparelli. M. A. Davies and A. E. Aplin are supported by Dr. Miriam and Sheldon G. Adelson Medical Research Foundation. Research reported in this publication utilized the Flow Cytometry, Translational Pathology, BioImaging, and Cancer Genomics Shared Resources at Sidney Kimmel Cancer Comprehensive Center at Jefferson Health, supported by the NCI/NIH under award number P30CA056036. A. T.

Weeraratna is supported by P01 CA114046, U01CA227550, R01CA232256, a Bloomberg Distinguished Professorship and the EV McCollum Endowed Chair. The content is solely the responsibility of the authors and does not necessarily represent the official views of the NIH. The RPPA studies were performed at the Functional Proteomics Core Facility at The University of Texas MD Anderson Cancer Center, supported by an NCI Cancer Center Support Grant (P30 CA16672).

ABSTRACT

Despite the clinical success of targeted inhibitors in cutaneous melanoma, therapeutic responses are transient and influenced by the aged tumor microenvironment, and drug-tolerant residual cells seed resistance. Given the similarities between drug tolerance and cellular dormancy, we studied the dormancy marker, nuclear receptor subfamily 2 group F member 1 (NR2F1), in response to targeted therapy. We utilized BRAF-V600E inhibitors (BRAFi) plus MEK inhibitors (MEKi) in *BRAF*-mutant melanoma models since melanoma patients treated with this combination display minimal residual disease, but ultimately tumors relapse. Transcriptomic analysis of melanoma samples from patients treated up to 20 days with BRAFi + MEKi showed increased expression of NR2F1. Similarly, NR2F1 was highly expressed in the drug-tolerant invasive cell state of minimal residual disease in patient-derived and mouse-derived xenograft tumors on BRAFi + MEKi treatment. Overexpression of NR2F1 alone was sufficient to reduce BRAFi + MEKi effects on tumor growth *in vivo* as well as on cell proliferation, death, and invasion *in vitro.* NR2F1-overexpressing cells were enriched for hallmarks gene sets for mTORC1 signaling, and NR2F1 bound to the promoter regions of genes involved in mTORC1 signaling. These cells were sensitive to the combination of BRAFi, MEKi plus rapamycin *in vitro* and *in vivo*. Melanomas from aged mice, which are known to exhibit a decreased response to BRAFi + MEKi, displayed higher levels of NR2F1 compared to tumors from young mice. Depleting NR2F1 levels in an aged mouse melanoma model improved the response to targeted therapy. These findings show high NR2F1 expression in 'invasive-state' residual cells and that targeting NR2F1-high cells with mTORC1 inhibitors could improve outcomes in melanoma patients.

INTRODUCTION

Current standard-of-care treatments for melanoma, including immune checkpoint inhibitors and mitogen-activated kinase pathway (MAPK) targeted therapies, are limited by innate and acquired resistance (2, 3). For patients with *BRAF*-mutant melanoma, combination treatment with BRAF inhibitors and MEK inhibitors (BRAFi + MEKi) leads to tumor shrinkage in the majority of patients (2), but tumors progress with a median progression-free survival (PFS) of approximately 14 months (4). Therapy response is modulated by the tumor microenvironment (TME) (5, 6). In particular, the aged TME enhances tolerance to BRAFi + MEKi by preventing tumor cell death, increasing angiogenesis, and altering normal dermal fibroblasts to secrete factors that promote resistance (7, 8). Furthermore, older mice (>52 weeks) exhibit lower response rates to targeted therapy relative to younger mice (8 weeks) (7-10). In humans, ~50% of melanoma cases occur in individuals over the age of 50, with a median age of diagnosis of ~63 years (7, 8).

Minimal residual disease (MRD) is characterized by slow-cycling/quiescent drug-tolerant persister (DTP) cells (11, 12) and may form a reservoir of cells that seed acquired resistance (11, 13, 14). Some subpopulations of DTP cells have invasive potential and may generate lesions at distant sites that grow out several years after treatment (1, 15, 16). Both tumor cell dormancy and MRD following BRAFi + MEKi are associated with progression (17, 18), and several drug tolerance mechanisms have been identified (13, 19). AXL overexpression and MITF/SOX10 loss promote the survival of drug-tolerant cells (11), associated with transcriptional reprogramming that drives a proliferative-to-invasive phenotype switch (20, 21). Additional transcriptomic states of DTP cells exist (22-25) including a dormancy gene signature associated with activation of stress-signaling pathways such as p38 kinase and PRKR-like endoplasmic reticulum kinase (PERK) (24, 26). A better understanding of DTP cells is key for effectively preventing acquired resistance in metastatic melanoma.

Disseminated tumor cells that have migrated to metastatic sites but remain dormant exhibit similar properties to DTPs (6, 27). Expression of the orphan nuclear receptor subfamily 2

group F member 1 (NR2F1, also known as COUP-TFI) promotes tumor cell dormancy via induction of SOX9/RARβ/TGFβ/p38-driven quiescence programs in breast and prostate tumor models (28, 29); however, the role of NR2F1 in drug tolerance remains unknown. Here, we show that NR2F1 is highly expressed in melanoma patient samples characteristic of the invasive subgroup of DTPs and in cell-derived xenografts in MRD following treatment with BRAFi + MEKi. Inducible overexpression of NR2F1 reduced BRAFi + MEKi efficacy in melanoma models *in vitro* and *in vivo.* Similarly, tumors from aged mice presented higher expression of NR2F1 than tumors from younger animals. NR2F1-expressing cells partially maintained mTORC1 signaling in the presence of BRAFi + MEKi and were sensitive to the mTORC1 inhibitor rapamycin in combination with BRAFi + MEKi. Together, our findings indicate that targeting DTP cells expressing high levels of NR2F1 may improve targeted therapy outcomes in melanoma.

RESULTS

NR2F1 is upregulated in melanoma tumors following BRAFi and MEKi therapy

NR2F1 is associated with tumor dormancy in several tumor models (28, 30) and the BRAFi + MEKi drug-tolerant state exhibits similar traits to cellular dormancy, prompting us to test the link between NR2F1 and targeted therapy response. First, we analyzed published RNA sequencing (RNA-seq) datasets from melanoma patients treated with BRAFi + MEKi (31-33). Sample expression and metadata were retrieved from the Gene Expression Omnibus (GEO), and analysis was limited to patients treated up to 20 days with the combination of BRAFi (dabrafenib) and MEKi (trametinib) (Fig. 1A). In both the Kwong et al. and Song/Hugo/Lo et al. datasets, NR2F1 mRNA levels were significantly higher ($p=0.033$ and $p<0.001$, respectively) in BRAFi + MEKi on-treatment samples compared to patient-matched pre-treatment samples (Fig. 1A). Using the Tsoi et al. melanoma drug-tolerant states dataset (34), we analyzed NR2F1 expression in the transition between phenotypic states and targeted therapy tolerance. NR2F1 expression was enhanced in the undifferentiated cell state (Fig. 1B), one of four melanoma states identified as highly invasive and resistant to BRAFi + MEKi. To further connect NR2F1, MRD and therapy tolerance, we analyzed the publicly available single-cell RNA-seq (scRNA-seq) dataset from Rambow et al. (13). This dataset compares four drug-tolerant states (neural crest stem cell, invasive, “starved”-like melanoma cell, and pigmented) that are present in MRD following BRAFi + MEKi in *BRAF*-mutant melanoma patient-derived xenografts (PDXs). NR2F1 was selectively upregulated in the MRD-invasive state of DTP cells (Fig. 1C and Supp. Fig. S1A).

Additionally, NR2F1 expression was assessed in the Song/Hugo/Lo et al. study, which compares transcriptomes of patient-derived tumors on targeted therapy to MAPKi-induced cell states in human melanoma cell lines. The dynamic transcriptomic states are defined as subpopulations of DTP, DTP proliferating cells (DTP-Prolif); and BRAFi/MEKi- or BRAFi/MEKi/ERKi-resistant sublines after short-term (2 days) or long-term (weeks/months)

144 treatment (33). Using average expression data taken from this study, we observed that NR2F1
145 levels were increased after MAPK pathway inhibition in *BRAF*-mutant cell lines independently of
146 their dynamic transcriptomic states (Supp. Figs. S1B-C) (33). Together, these data suggest that
147 NR2F1 is expressed in melanoma patient tumors in MRD.

148 To test the association of NR2F1 with MRD in pre-clinical models, we identified cell lines
149 with detectable NR2F1 expression (Supp. Fig. S1D) and treated xenografts from the NR2F1-
150 expressing *BRAF*-mutant 1205Lu cell line, with BRAFi (PLX4720) and MEKi (PD0325901). As
151 expected, BRAFi + MEKi caused tumor regression leading to MRD by 3 weeks (Fig. 1D). NR2F1
152 levels were enriched in MRD xenografts on BRAFi + MEKi compared to control tumors as
153 detected by immunofluorescence at 3 week post-treatment MRD time point (Fig. 1E and Supp.
154 Fig. S1E). Additionally, we probed for the expression of NR2F1 in BRAFi + MEKi-tolerant cell
155 lines that we have previously described (25, 35). Publicly accessible RNA-seq analysis (25)
156 showed increased mRNA expression of NR2F1 in two A375 BRAFi + MEKi tolerance models,
157 CRT34 and CRT35, compared to parental A375 cells (Supp. Fig. S1F). Additionally, there was a
158 modest but detectable increase in protein expression of NR2F1 in CRT34 and CRT35 cells
159 cultured in the presence/absence of BRAFi + MEKi for 24 hours compared (Supp. Fig. S1G).
160 Together, these data associate NR2F1 upregulation with drug tolerance and MRD following
161 targeted therapy in cutaneous melanoma.
162
163 **NR2F1 overexpression minimizes tumor inhibition effects by BRAFi and MEKi treatment**
164 To determine whether NR2F1 is sufficient to enhance drug tolerance, we induced the expression
165 of NR2F1 in *BRAF*-V600E 1205Lu, WM793, and A375 melanoma cell lines and treated
166 with/without BRAFi + MEKi (Fig. 2A). LacZ/beta-galactosidase was used as a control for the
167 inducible protein expression system (Supp. Fig. S2A). No other members of the NR2F family were
168 upregulated when NR2F1 was overexpressed in melanoma lines (Supp. Fig. S2B). In colony
169 growth assays, inducible expression of NR2F1 did not alter melanoma cell growth in the absence

of BRAFi + MEKi but was able to partially rescue colony growth in the presence of BRAFi + MEKi (Fig. 2B and Supp. Fig. S2C). We further tested whether NR2F1 expression altered cell proliferation following BRAFi + MEKi by measuring S-entry phase using 5-ethynyl-2'-deoxyuridine (EdU) staining. BRAFi + MEKi-treated cells that overexpressed NR2F1 exhibited higher EdU staining than non-NR2F1-overexpressing cells on targeted therapy (Fig. 2C). Additionally, as BRAFi + MEKi induces cell death (36), we tested whether NR2F1 overexpression impacted cell death by measuring propidium iodide (PI) uptake via real-time IncuCyte analysis. NR2F1 overexpression significantly reduced PI uptake during BRAFi + MEKi (Fig. 2D).

Since drug-tolerant cells may also gain motility and interact with the extracellular matrix to promote disease progression (37, 38), we investigated how NR2F1 influences tumor invasion. Using a 3D tumor spheroid outgrowth assay, NR2F1 expression enhanced melanoma invasiveness in spheroids treated with BRAFi + MEKi (Fig. 2E and Supp. Fig. S2D). To confirm that NR2F1 confers a survival benefit to melanoma cells in the presence of BRAFi + MEKi, we inducibly expressed either tdTomato-NR2F1-WT or a dominant-negative form of NR2F1, GFP-NR2F1-C141S in 1205Lu-TR and WM793TR, Tet Repressor-expressing melanoma cells. NR2F1-C141S harbors a point mutation within its DNA binding domain (39). When co-cultured at a 1:1 ratio, tdTomato-NR2F1-WT cells outgrew the GFP-NR2F1-C141S mutant cells in the presence of BRAFi + MEKi (Fig. 2F-G). In sum, our data suggest that NR2F1 confers a pro-growth and pro-invasion state in melanoma during targeted therapy treatment.

Despite presenting a Response Evaluation Criteria in Solid Tumours (RECIST)-defined complete response to MAPK inhibitors (40), residual disease often persists and approximately 80% of patients progress (41-43). Thus, we tested whether NR2F1-expressing cells tolerate long periods of targeted therapy treatment. Real-time IncuCyte monitoring of cell growth confirmed the ability of NR2F1-overexpressing cells to maintain growth following a 28-day exposure to BRAFi + MEKi across multiple melanoma lines (Fig. 3A). *In vivo*, xenografts overexpressing NR2F1 responded to BRAFi + MEKi treatment but progressed faster over time than non-induced tumors

(Fig. 3B-C). Mice harboring tumors overexpressing NR2F1 showed poorer survival than mice bearing control xenografts on targeted therapy treatment (Fig. 3D). Together, these data suggest that *BRAF*-mutant melanoma cells expressing high levels of NR2F1 tolerate targeted therapy and tumors display a shorter time to resistance.

NR2F1 expression leads to enrichment of growth-related transcripts following BRAFi and MEKi therapy

To investigate how NR2F1 may lead to targeted therapy tolerance, we performed bulk RNA-seq and gene set enrichment analysis (GSEA) on melanoma cells treated with BRAFi + MEKi with/without NR2F1 overexpression. In three melanoma cell lines (1205Lu, WM793, and A375), NR2F1 expression induced an enrichment in the hallmark gene sets for MYC targets variant 2 and mTORC1 signaling in the presence BRAFi + MEKi compared to treated controls that do not overexpress NR2F1 (Fig. 4A-B and Supp. Fig. S3A). NR2F1 overexpression also increased enrichment in the hallmark gene sets for late response to estrogen (Supp. Fig. S3B). Some pathways were only altered in 2 out of 3 cell lines. For example, enrichment hallmark gene sets for MYC targets variant 1, DNA repair, E2F targets, G2/M checkpoint, mitotic spindle, and spermatogenesis were upregulated in NR2F1-expressing 1205Lu and A375 cells (Supp. Fig. S3C); whereas augmenting cholesterol homeostasis, unfolded protein response, interferon-alpha response, interferon-gamma response, and hypoxia were altered in 1205Lu and WM793 (Supp. Fig. S3D). Additionally, we observed an NR2F1-dependent reduction in an adipogenesis gene set in WM793 and A375 cell lines (Supp. Fig. S3E).

Given the role NR2F1 in dormant and senescent cancer cells (28, 29), we further queried these RNA-seq data with dormancy “down” and “up” gene signatures from Kim et al. (44). We found no consistent significant changes in dormancy markers (other than NR2F1) across all cell lines comparing BRAFi + MEKi treatment -/+ NR2F1 overexpression (Supp. Fig. S3F-H). For example, ADAM10 from the “up” signature is significantly decreased in 1205Lu and WM793 cells,

but increased in A375 cells. In the dormancy “down” signature, CDKN3, CKS2, BUB1, FOXM1, BUB1B, and TK1 are all significantly increased in 1205Lu and WM793 cells, but either go up or down (not significantly) in A375. We further probed additional dormancy markers from Fane et al. (9), again finding significant changes in only 2 of 3 cell lines (for example, increased DKK1 in A375 and WM793 cells) (Supp. Fig. S3G). Next, to address the possible role of NR2F1 overexpression on senescence, we queried these RNA-seq data with the REACTOME Cellular Senescence gene pathway, finding that only IL-6 was significantly increased in all cell lines (Supp. Fig. S3H). Together, these data suggest that NR2F1 overexpression impacts multiple components of dormancy, but not always consistently between cell lines, in melanoma models on BRAFi + MEKi treatment.

As we observed increased S-phase entry of NR2F1-overexpressing cells during BRAFi + MEKi (Fig. 2C), we probed the RNA-seq data for the KEGG cell cycle gene signature in all cell lines. GSEA analysis of the KEGG cell cycle pathway displayed a positive enrichment of cell cycle genes with NR2F1 overexpression in BRAFi + MEKi-treated cells (Supp. Fig. S3I). We probed for genes that were altered during NR2F1 overexpression in BRAFi + MEKi-treated cells and found that numerous genes were significantly upregulated in 2 of 3 cells lines. For example, CDKN1A was only significantly increased in 1205Lu and WM793 cells, while MCM genes, CDC genes, ORC genes, BUB genes, and others were only significantly increased in 1205Lu and A375 cells (Supp. Fig. S3J). Thus, NR2F1 overexpression has a restorative effect on multiple components of the cell cycle during BRAFi + MEKi.

In parallel to RNA-seq analyses, we tested the effect of NR2F1 on survival-related signaling pathways by reverse-phase protein array (RPPA) analysis. Consistent with RNA-seq and GSEA results (Figs. 4A-B, and Supp. Fig. S3), NR2F1-overexpressing melanoma cells treated with BRAFi + MEKi displayed high mTORC1 pathway readout (phospho-S6), higher expression of cell cycle and survival regulators such as cyclin B1, PLK1, phospho-RB1, phospho-S6, and Wee1, than BRAFi + MEKi-treated non-NR2F1-overexpressing cells (Fig. 4C). Altered

levels of RPPA-identified proteins involved in cell cycle and survival were validated by Western blot and subsequent quantification (Fig. 4D and Supp. Fig. S4A) (44). Overall, our data indicate that NR2F1 maintains cell growth in drug-tolerant melanoma on targeted therapy, in part, through enhancing the level of mTORC1 signaling during BRAFi + MEKi treatment.

To further assess NR2F1 modulation of mTORC1 signaling, we queried the RNA-seq data and identified commonly enriched genes in the Hallmark mTORC1 gene set for 3 independent cell lines overexpressing NR2F1 and treated with BRAFi + MEKi. We found 21 significantly overlapping genes (Supp. Fig. S4B) involved in the mTORC1 pathways, such as PDK1 and HSPD1, that were upregulated in the presence of NR2F1 overexpression during BRAFi + MEKi treatment (Fig. 4E). We then queried publicly available MACS2 (45) NR2F1 ChIP-seq binding data from the Gene Transcription Regulation Database (46) and identified that NR2F1 bound to the promoter region of 17 of the 21 genes identified including PDK1 and HSPD1 (Fig. 4F). Together, these data suggest that mTORC1 signaling is partially rescued after NR2F1 upregulation during BRAFi + MEKi treatment, likely by NR2F1 binding to the promoter region of genes that promote mTORC1 signaling and inducing their transcription.

Targeting mTORC1 decreases MRD during BRAFi + MEKi treatment

A previous study has shown that inhibition of mTORC1 signaling delays the onset of acquired resistance to BRAFi and/or MEKi (47). Based on the partial maintenance of mTORC1 signaling, we tested the efficacy of two mTOR inhibitors (AZD2014 and rapamycin) to target NR2F1-overexpressing cells (48). In NR2F1-induced cells, mTORi alone did not affect growth; however, a triple combination using BRAFi + MEKi + mTORi prevented colony formation (Fig. 5A). Real-time monitoring assays of cell growth over three weeks indicated that NR2F1-overexpressing cells responded better to the triple combination treatment (Fig. 5B), suggesting a potential therapeutic strategy to target DTP melanoma cells. Western blot analysis showed that mTORi inhibited phospho-S6 levels in NR2F1-overexpressing cells on BRAFi + MEKi (Supp. Fig. S5A),

further supporting our proposed model whereby DTP cells are associated with NR2F1 overexpression and persistent mTOR signaling.

We tested the effect of mTORi on residual tumors following BRAFi + MEKi *in vivo*. Despite using an intermittent regimen of 2 days on/5 days off AZD2014 administered with continuous BRAFi + MEKi, we had to interrupt our initial *in vivo* experiments due to symptoms of drug toxicity, including lethargic behavior and ≥20% of body weight loss in triple combination-treated animals (Supp. Fig. S5B). To manage toxicity while retaining efficacy, we tested a combined BRAFi + MEKi + rapamycin treatment for one week in MRD tumors. Rapamycin (sirolimus) is well tolerated in xenograft models and in patients on clinical trials (49, 50). NR2F1 levels were downregulated in MRD xenografts following BRAFi + MEKi + rapamycin compared to BRAFi + MEKi-residual tumors as detected by immunofluorescence (Fig. 5C and Supp. Fig. S5C).

Given these promising results with rapamycin, we tested the effects of BRAFi + MEKi + rapamycin compared to BRAFi + MEKi, by treating mice with rapamycin twice a week to avoid potential toxicity. Tumors were initially treated with BRAFi + MEKi. Upon reaching MRD when tumors express high NR2F1 (Fig. 1E and 5C) and tumor size is stable for several weeks, rapamycin was given in combination with BRAFi + MEKi. Rapamycin delayed tumor regrowth during BRAFi + MEKi, but did not significantly impact mouse weight compared to BRAFi + MEKi alone (Fig. 5D-E and Supp. Fig. S5D). Specifically, for mice with tumors that regrew to 100 mm^3, the exponential regrowth rates in each treatment group and the difference in the regrowth rates between BRAFi + MEKi + rapamycin versus BRAFi + MEKi groups were estimated (Fig 5E). Tumors in BRAFi + MEKi + rapamycin group grew significantly slower ($p=0.0005$) with a 3% daily increase (95% CI: 2.1-3.9%) versus a 5.2% daily increase (95% CI: 4.4-6.1%) in the BRAFi + MEKi group. Altogether, these data suggest that inhibiting mTORC1 with rapamycin treatment improves targeted inhibitor therapy by targeting DTP melanomas that overexpress NR2F1 and decreasing regrowth rates from MRD.

NR2F1 is overexpressed in aged *BRAF*-mutant melanoma models

Age is an important poor prognostic factor in melanoma patients (51, 52). Indeed, older patients and aged pre-clinical mouse models with melanoma exhibit poor response to targeted therapy relative to younger patients/mice due to drug resistance mediated by the aged TME (7, 8). Aged dermal fibroblasts promote melanoma metastasis and resistance to BRAFi + MEKi therapy (7). Specifically, tumors grow more quickly and BRAFi + MEKi rapidly loses efficacy in mouse melanoma models in aged mice compared to young mice (9, 10). Since the majority of patients diagnosed with melanoma are above 66 years old and older individuals with melanoma respond worse to BRAFi + MEKi treatment than younger people, we assessed whether NR2F1 expression was differentially affected by an aged TME using aged mice.

Melanoma cells cultured in conditioned medium (CM) derived from skin fibroblasts isolated from aged healthy human donors (>55 years old) expressed a higher level of NR2F1 compared to cells cultured in young donor (<35 years old) fibroblast-derived CM (Fig. 6A). These data were supported by findings in intradermally-injected allograft primary tumors borne in aged mice (>52 weeks) that expressed higher levels of NR2F1 by immunohistochemistry staining compared to tumors borne in young mice (8 weeks) (Fig. 6B and Supp. Fig. S6); tumor sizes were over ~500 mm^3 in young and aged mice (9). These data indicate that NR2F1 expression is increased in melanoma cells surrounded by an aged TME.

BRAFi + MEKi therapy is less effective in subcutaneous or intradermal tumors in an aged microenvironment (7, 9, 10). To assess the relevance of high NR2F1 expression in determining the poor response to BRAFi + MEKi in aged mice, we directly targeted NR2F1 using a tetracycline-inducible short hairpin RNA (shRNA) (Fig. 6C). In aged mice, partial knockdown of NR2F1 elicited no effect on tumor growth in the absence of inhibitors but enhanced the effect of BRAFi + MEKi on tumor growth and delayed the time to disease progression (Fig. 6D). Associated with these effects, animal survival was increased in the presence of BRAFi + MEKi treatment with NR2F1 knockdown (Fig. 6E). These data suggest that NR2F1 is upregulated in tumors residing

in an aged TME and that reducing NR2F1 enhances the effects of BRAFi + MEKi treatment in an aged mouse melanoma model.

DISCUSSION

Therapeutic responses to targeted inhibitors are frequently transient and tumors regrow from a reservoir of slow-cycling cells that survive initial treatment (53). Here, we describe that NR2F1 plays a role in the survival of drug-tolerant melanoma lesions. NR2F1 is upregulated in residual xenografts following BRAFi + MEKi treatment. Analysis of publicly available datasets (13, 31, 33) also revealed increased NR2F1 expression in both patient and MRD lesions from PDX samples on BRAFi + MEKi treatment. NR2F1-overexpressing cells were more tolerant to BRAFi + MEKi treatment and displayed higher expression of cell growth markers, phospho-RB1 and phospho-S6. *BRAF*-mutant melanomas that emerge from an aged TME, known to be less sensitive to BRAFi + MEKi (7), also upregulated NR2F1 protein levels. Targeting BRAFi + MEKi-tolerant cells that overexpress NR2F1 using the mTOR inhibitor rapamycin delayed melanoma regrowth and the emergence of resistance (Fig. 7).

Dormancy and drug tolerance have been linked to resistance and disease relapse in melanoma (16, 17, 54-56); therefore, we questioned whether NR2F1 contributes to BRAFi + MEKi tolerance and the persistence of MRD burden. Our finding that NR2F1 is upregulated in patients and mouse melanoma residual tumors on BRAFi + MEKi treatment are consistent with studies that identified dormant marker expression in cells in the MRD state (57). Furthermore, high expression of NR2F1 is associated with tumor relapse and metastasis in salivary adenoid cystic carcinoma, urothelial cancer, and renal cancer models (58, 59). NR2F1 overexpression is reported to upregulate SOX9 through RAR-beta (28); SOX9 overexpression has been linked to promoting migration, metastasis, and resistance to targeted therapy in melanoma (60, 61). Additional studies are warranted to determine how NR2F1 might play a role in maintenance of drug-tolerant melanoma cells.

To investigate how NR2F1 is involved in drug-tolerant persistence, we overexpressed NR2F1 in melanoma lines. Both *in vitro* and *in vivo* results showed a higher tumor growth rate in NR2F1-overexpressing cells following BRAFi + MEKi treatment. Our transcriptomic and

proteomic analyses determined that NR2F1 overexpression led to maintenance of mTORC1 pathway activation on BRAFi + MEKi treatment. Others have also shown that cell proliferation and PI3K/AKT/mTORC1 signaling are restored following resistance to BRAFi + MEKi therapy (62-64). NR2F1 has been previously reported to induce tumor dormancy and inhibit mTOR signaling in several cancer models (28, 30, 57, 65-68). On the other hand, high levels of NR2F1 may promote proliferation, invasion, and AKT/mTOR signaling activation via NR2F1-AS1, a long non-coding RNA with oncogenic characteristics (69, 70). NR2F1-AS1 was found to activate NR2F1 in esophageal squamous cell carcinoma to promote cancer progression by activating the hedgehog signaling pathway (69). In our study, while expression of NR2F1 alone did not inhibit cell proliferation, invasion, or mTOR signaling in our models, NR2F1 did partially rescue mTORC1 signaling in BRAF/MEK-targeted cells. Importantly, we observed that NR2F1 bound the promoter region of 17 different genes involved in mTORC1 signaling. For example, NR2F1 bound PDK1, which activates mTORC1 by phosphorylation of TSC2, thus its overexpression could be upregulating mTORC1 signaling and activity (71). Furthermore, NR2F1 bound HSPD1, which can stabilize ATP5A1 in cancer cells, leading to activation of mTOR signaling (72). Future studies will determine how the binding of NR2F1 to the promoter region of various genes involved in mTORC1 signaling relates to the findings of this manuscript.

The 'invasive state' is a characteristic of dedifferentiated DTP cells emerging during targeted therapy of melanoma (22). We showed that NR2F1 expression is selectively upregulated in the invasive (13) and undifferentiated cell states (34). Furthermore, NR2F1 is sufficient to promote invasion in the presence of BRAFi + MEKi *in vitro*. Our data are consistent with studies that showed that both the invasive and undifferentiated cell states exhibit a highly invasive phenotype and intrinsic tolerance to MAPK inhibition (22, 34, 73, 74). Others have shown that overexpression of NR2F1 increases invasiveness and metastatic potential in tumor and cancer-associated stromal cells (65, 68). For instance, salivary adenoid cystic carcinoma cells had increased expression of CXCL12 and CXCR4, enhanced invasion, and metastasis after

overexpression of NR2F1; knockdown of NR2F1 reduced the invasive phenotype in these cancer cells (65). Thus, NR2F1 may modulate the invasive behavior of residual cells.

We also tested whether mTORC1 inhibitors could selectively target residual cells overexpressing NR2F1. *In vitro*, both the mTORC1/2i, AZD2014, and the mTORC1i, rapamycin, inhibited growth of NR2F1-overexpressing cells, indicating that targeting mTORC1 may delay melanoma relapse. However, increased toxicities in MRD-bearing mice limited the *in vivo* efficacy of BRAFi + MEKi + AZD2014. AZD2014 inhibits AKT activation, which may lead to increased toxicity *in vivo* (75). We tested a BRAFi + MEKi + rapamycin treatment regimen for better tolerability to target NR2F1-overexpressing cells. BRAFi and MEKi suppress mTOR signaling initially, but the pathway rebounds after tumors become resistant (47, 48, 50). Thus, targeting drug-tolerant cells that overexpress NR2F1 using mTORi may prevent the rise of drug-resistant subpopulations. Importantly, our findings show that a triple combination of BRAFi + MEKi + mTORi inhibits the survival of NR2F1-overexpressing cells *in vivo* and decreases tumor regrowth rates from MRD, suggesting that mTORi delays tumor growth of DTP cells.

Aging can negatively affect melanoma patient prognosis due to aged tumors being more invasive and less responsive to targeted therapy (5, 7, 8, 76). NR2F1 is upregulated in the aged dermal TME compared to younger dermal TME. We also examined the expression levels of NR2F1 in aged TME-derived melanomas and showed that knockdown of NR2F1 in aged tumor-bearing mice reduced growth and improved survival following BRAFi + MEKi. Importantly, a positive correlation exists between NR2F1 and genes associated with the 'invasive' $Wnt5A^{high}/AXL^{high}$ signature of melanoma tumors surrounded by an aged TME (9). The secretome of young and aged skin human fibroblasts has been previously defined (77) and the authors found numerous changes (90 proteins with significant up- or down-regulation) related to aged fibroblasts. Retinoic acid receptor responder protein-2 (RARRES2) was increased in aged fibroblasts and NR2F1 can be regulated by retinoic acid signaling (28). Thus, one possibility for future testing is that secreted RARRES2 impacts the expression of NR2F1 in these tumors.

Midkine has also been implicated in modulating NR2F1 (78), but the aforementioned secretome data show that midkine is decreased in aged fibroblasts, likely ruling out this mechanism. The regulation of NR2F1, especially by secreted factors, is not fully understood and addressing this question in depth is an ongoing area of research.

Aligned with evidence that aged skin fibroblasts stimulate melanoma invasion, metastasis, and resistance to BRAFi via increased secretion of SFRP2 into the TME (5, 7, 79, 80), our data suggest that aged tumors are less likely to benefit from BRAFi + MEKi therapy due to their high levels of NR2F1, which cooperates with the aged TME to drive drug tolerance. Given the additive effects of rapamycin on BRAFi + MEKi treatment we observed in this study, treating older patients with this triple combination therapy may circumvent NR2F1-driven BRAFi + MEKi drug tolerance in the aged TME, as long as toxicity can be avoided.

Studying drivers of MRD and drug tolerance may help identify vulnerabilities that can be exploited therapeutically in combination with BRAFi + MEKi to delay melanoma relapse. Further research is needed to confirm these findings in other cancer types upon MAPK inhibition and investigate the role of NR2F1 in immunocompetent models. Our results suggest that targeting NR2F1 in concert with BRAFi + MEKi will likely promote more durable responses to targeted therapy for BRAF-mutant melanoma *in vivo*.

MATERIAL AND METHODS

Sex as a biologic variable: For human xenograft mouse experiments, we used equal numbers of males and females to control for any sex differences. For the experiments using YUMM1.7 tumors, only male mice were used as this is a syngenic tumor model derived from a male mouse, and, thus would be rejected in female mice. More details can be found in “in vivo experiments”.

Cell culture: 1205Lu and WM793 human melanoma cells (donated by Dr. Meenhard Herlyn, The Wistar Institute, Philadelphia, PA, in 2005) were cultured in MCDB 153 medium containing 20% Leibovitz-L15 medium, 2% fetal bovine serum (FBS, Life Technologies; Grand Island, NY), 0.2% sodium bicarbonate, and 5 μg/mL insulin. A375 human melanoma cells (purchased from ATCC in 2005) were cultured in Dulbecco's modified Eagle's medium (DMEM, GIBCO, Life Technologies) supplemented with 10% FBS. A375 BRAFi + MEKi tolerant cell lines, CRT34 and CRT35, were previously generated and characterized (25, 35). All cell lines used in this study were validated as BRAF-V600 mutated by Sanger sequencing. YUMM1.7 mouse melanoma cells were cultured in DMEM/F12 with 10% FBS and 1% non-essential amino acids. All cells were grown with 1% penicillin/streptomycin added to all media at 37°C in 5% CO_2. Human cell lines were authenticated by STR analysis. Cells were routinely assayed for mycoplasma contamination with MycoScope Kit (Genlantis; San Diego, CA).

Inhibitors and reagents: The inhibitors PLX4720 (BRAF inhibitor), PD0325901 (MEK inhibitor), and AZD2014 (mTORC1/2 inhibitor) were purchased from Selleck Chemicals LLC (Houston, TX). Doxycycline hyclate (82D9891) was purchased from Sigma-Aldrich (St. Louis, MO). For *in vivo* experiments, PLX4720 and PD0325901 were kindly provided by Plexxikon Inc. (Berkeley, CA). The published structures for the inhibitors used in this manuscript are provided in Supp. Fig. S7.

Lentiviral construction and transduction: 1205LuTR, WM793TR, and A375TR Tet repressor expressing, doxycycline-inducible LacZ-overexpressing cells were previously generated (81). Transgene expression was induced with DOX, as indicated (100 ng/mL). Human NR2F1-WT and NR2F1-C141S were amplified from aVsir (NM_028732) expression plasmid (OriGene; Rockville, MD), cloned into pENTR/D-TOPO (Invitrogen; Carlsbad, CA), and LR recombined into pLenti-4/TO/V5-DEST. Expression constructs and packaging plasmids pLP1, pLP2, and pLP/VSVG were co-transfected into Lenti-X 293T cells (Takara Bio Inc., Shiga, Japan) to generate viral particles. Cells were transduced with particles for 48 hours and then selected with hygromycin, as previously described (81).

Generation of fluorescent-labeled cells: For tdTomato labeling, 1205LuTR and WM793TR cells were previously transduced with tdTomato fluorescent protein (82), and highly expressing cells were sorted. A similar approach was followed for GFP labeling of 1205LuTR and WM793TR, except that the pLV-eGFP (#36083, Addgene) plasmid was used.

Western blot analysis: Protein lysates were prepared in Laemmli sample buffer, separated by SDS-PAGE, and proteins transferred to PVDF membranes. Immunoreactivity was detected using horseradish peroxidase-conjugated secondary antibodies (CalBioTech; Spring Valley, CA) and chemiluminescence substrate (Thermo-Scientific; Waltham, MA) on a Versadoc Imaging System (Bio-Rad; Hercules, CA). The primary antibodies used were as follows: COUP-TFI/NR2F1 (#6364), phospho-RB1 (S780, #9307), phospho-RB1 (S807/811, #9308), RB (#9309), phospho-S6 (S235/236, #4857), phospho-S6 (S240/244, #2215), S6 ribosomal protein (#2217), FOXM1 (#5436), Aurora A/AIK (#3092), PLK1 (#4513), Wee1 (#4936), and RSK1 (#9333) from Cell Signaling Technology (Danvers, MA); and vinculin (sc-73614) from Santa Cruz Biotechnology Inc. (Dallas, TX).

Reverse-phase protein array (RPPA) analysis: Cells were seeded in 6-well plates in media with DOX for 24 hours to induce NR2F1-WT expression. The day after, cells were treated with DMSO, BRAFi + MEKi (PLX4720 1 μmol/L + PD0325901 35 nmol/L) + DOX (100 ng/mL) for an additional 72 hours. RPPA analysis was performed at the MD Anderson Functional Proteomics Core Facility (Houston, TX), and the data were used to determine antibodies significantly different between -/+ BRAFi + MEKi and -/+ DOX treated groups for each cell line, as previously described (83). Relative protein levels were quantified using SuperCurve fitting and normalized for protein loading. Comparison of average normalized $\log_2$ values was performed by the two-sample t-test method with 1,000 permutations and assumed unequal variance. Antibodies with a p-value <0.05 were considered significant. Statistical calculations were performed in MATLAB® (v2015b) using the mattes function. Data points are shown as averages of three experimental replicates.

RNA sequencing sample preparation and analysis: 1205LuTR-NR2F1, WM793TR-NR2F1, and A375TR-NR2F1 cells were seeded in 6-well plates in regular growth media and with DOX for 24 hours to induce NR2F1-WT expression. The day after, cells were treated with DMSO (control), -/+ BRAFi + MEKi (in combination, PLX4720 1 μmol/L + PD0325901 35 nmol/L), and -/+ DOX (100 ng/mL) for an additional 72 hours. Total RNA was isolated using the RNeasy Plant Mini Kit (QIAGEN; Hilden, Germany). Raw RNA-seq reads were aligned to the GRCh38 human reference genome using the Star (v2.7.0) method (84) and GENCODE (v35) (85) annotations. RSEM (v1.2.28) (86) was used to quantify gene and transcript-level expression, while gene normalization and differential expression analyses were performed using DESeq2 (v1.28.1) (87). For each cell line, a '.gct' file with normalized expression data was generated using the cMap (v1.4.0 https://github.com/cmap/cmapR) package after removing genes with no expression. GSEA (v4.1.0) (85, 88) was performed to identify significantly altered gene sets in the MSigDB Hallmark collection (v7.2) (88). The "Signal2Noise" weighted enrichment statistic was performed after collapsing from Ensembl to human gene identifiers. One thousand permutations were performed

using gene sets, and FDR q-values equaling zero are reported as less than 0.001. Heatmaps were generated using the pheatmap (v1.0.12 https://CRAN.R-project.org/package=pheatmap) package. Analyses were performed in R (v4.0.2 https://www.R-project.org/). The GEO accession number for the RNA-seq dataset from this study is GSE228600.

NR2F1 ChIP-seq binding: NR2F1 ChIP-seq data were evaluated for potential regulation of commonly enriched mTOR genes in multiple cancer types. MACS2 (45) ChIP-seq binding results for experiments targeting NR2F1 (n=5) were obtained from the Gene Transcription Regulation Database (GTRD) (46). Gene regulation data with promoter-transcript matches were obtained from Ensembl (v113) (89) for the human reference genome build GRCh38. Statistically significant MACS2 peaks (padj < 0.05) were used for identifying overlaps between promoter regions with annotated binding to the commonly enriched mTOR genes. Overlapping regions between MACS2 peaks and Ensembl regulatory elements was conducted using the GenomicRanges (v1.52.0)(90), rtracklayer (v1.60.1) (91) and GenomeInfoDb (v1.36.3 https://bioconductor.org/packages/GenomeInfoDb) packages. Heatmaps were generated using the pheatmap package (v1.0.12 https://CRAN.R-project.org/package=pheatmap). Data were analyzed in R (v4.3.2 https://www.r-project.org) via Rstudio (v2023.6.1 http://www.posit.co).

Immunofluorescence assay: Paraffin-embedded sections from human melanoma xenograft tumors were stained, as described (24). Briefly, samples were stained for protein expression after quenching endogenous peroxidase activity and blocked with PBS containing 3% normal goat serum. Binding of the primary antibody was carried out at 4°C overnight and detected by fluorescence-conjugated secondary antibody (1 hour at room temperature). Paraffin-embedded sections were stained for the following antigens: COUP-TFI/NR2F1 (ab181137, Abcam; Cambridge, MA) at 1:500 dilution; and vinculin (sc-73614, Santa Cruz Biotechnology Inc.) at 1:200 dilution. 4′,6-diamidino-2-phenylindole (DAPI) was used as DNA staining.

S-phase entry analysis: Cells were cultured in 6-well plates and treated. The thymidine analog EdU was added at a final concentration of 10 μmol/L for the last 16 hours of treatment. EdU incorporation was measured using the Click-iT Plus EdU Alexa Fluor 647 Flow Cytometry Assay Kit (Thermo Fisher Scientific) and was utilized per the manufacturer's instructions. EdU staining was analyzed on BD FACS LSRII Flow Cytometer (BD Biosciences; Franklin Lakes, NJ) using FlowJo software (TreeStar; Ashland, OR). Data points are shown as averages of three experimental replicates.

Crystal violet assay: Cells were seeded in 6-well plates and treated with either DMSO or BRAFi + MEKi (PLX4720 1 μmol/L + PD0325901 35 nmol/L) and +/- DOX (100 ng/mL) for one week. Media with drug treatments were replaced every two days. Cells were washed with PBS and stained with 0.2% crystal violet in 10% buffered formalin for 20 minutes. Subsequently, wells were washed and air-dried. Plates were scanned, and pictures were taken with a Nikon Eclipse Ti inverted microscope with NIS-Elements AR 3.00 software (Nikon; Melville, NY). Analysis was performed, as described previously (83).

IncuCyte® analysis: For real-time cell confluency quantification, cells were trypsinized and plated onto a 24-well plate. Photomicrographs were taken every 2 hours using an IncuCyte® Live cell imager (Essen Biosciences; Ann Arbor, MI). Plate confluence was measured using IncuCyte® software and presented as percentages. Propidium iodide (PI) uptake measurements were derived by dividing the PI-positive area ('surface fit' segmentation, RCU threshold = 0.75) by cellular confluence area ('AI Confluence' segmentation).

Tumor spheroid invasion assay: For 3D tumor spheroid formation, cells were plated in a 1.5% agar bed (w/v) for three days, as previously described (92). Then, 3D spheroids were embedded into collagen I solution. The next day, collagen-embedded 3D tumor spheroids were treated with

either DMSO or BRAFi + MEKi (PLX4720 1 μmol/L + PD0325901 35 nmol/L) and +/- DOX (100 ng/mL) for 72 hours. Cells were incubated with calcein-AM solution to mark live cells. Pictures were obtained using a Nikon A1R confocal microscope (Nikon). The area of the invasive front was quantified using ImageJ and normalized to the area of the spheroid.

In vivo experiments: For xenograft experiments, athymic mice (NU/J, homozygous, 6-8 weeks, 20-25 g, stock #002019, Jackson Laboratory; Bar Harbor, ME) were injected with 1205LuTR-E2F-tdtW-NR2F1 human melanoma cells. For allograft experiments, YUMM1.7-TetR-shNR2F1 ($2.5x10^5$ cells) were injected intradermally into aged male C57BL/6 mice (>52 weeks) (Charles River Laboratories; Willmington, MA). Mice bearing 1205Lu reporter xenografts or YUMM1.7 allografts (50-100 mm^3) were randomly divided into four cohorts and fed either control (AIN-76A diet) or BRAFi + MEKi (PLX4720 200 ppm + PD0325901 7 ppm)-laced chows (Research Diets Inc.; New Brunswick, NJ), -/+ DOX (25 mg/mL in water). Treatments were determined based on previous publications (35, 83). Xenograft cohorts had ten animals (5 females, 5 males) per group and allograft cohorts had ten animals (10 males) per group. For the triple combination study, mice bearing xenografts were fed with BRAFi + MEKi-laced chows or BRAFi + MEKi diet plus either with AZD2014 (administered by oral gavage bi-daily 2 days on/5 days off) (82), or with rapamycin 4 mg/kg (administered by i.p. daily). Cohorts had six animals (3 females and 3 males) per group. Control and combination chow arms received DMSO alone by oral gavage. Tumor volume measurements and animal survival were recorded every 2 to 3 days. Digital caliper measurements were used to calculate tumor volumes using the formula: volume = (length x $width^2$)/2. When approximately 10-15% of body weight loss was observed, diet gel 76A (ClearH2O; Westbrook, ME) was administered to minimize weight loss. Animals were sacrificed when tumors exceeded 1000 mm^3 (36, 83). To investigate the effects of rapamycin in combination with BRAFi + MEKi, mice bearing 1205Lu xenografts received BRAFi + MEKi chow until tumors regressed and reached a minimal residual disease state (stagnant growth for at least 2 weeks).

Treatment of BRAFi + MEKi chow plus 4mg/kg rapamycin or vehicle (administered i.p. twice weekly) was continued for the remainder of the experiment. Tumor volume and weight was measured every 3 to 4 days. To counteract weight loss, mice were provided diet gel 76A as a supplement. Animals were euthanized when tumors reached 700 mm^3.

Aged mice experiments were performed at the Johns Hopkins Bloomberg School of Public Health using C57BL/6 mice after 52 weeks of age. All animals were provided with food and water *ad libitum* and housed in cages of maximally 5. Mice were housed in sterile cages within laminar flow cage racks, and all were provided enrichment, such as nest-building materials. All mice were maintained under specific pathogen-free conditions in an AAALAC-approved Animal Facility at the Johns Hopkins University Bloomberg School of Public Health (Animal Welfare Assurance Number: A3272-01). The Johns Hopkins University Institutional Animal Care and Use Committee (IACUC) approved this protocol (MO22H405).

Patient RNA-seq datasets: For Song/Hugo/Lo's dataset (33), raw FASTQ sequencing reads for patient-derived tumor samples pre and early during treatment of BRAFi + MEKi were obtained from the Sequence Read Archive under the accession number SRP066571 using the SRA toolkit (v 2.10.4) (93). Reads were aligned to the GRCh38 human reference genome using Star method (84) and GENCODE v30 (85) annotations. RSEM (86) was used to quantify gene and transcript level expression. Normalization of gene expression was performed using DESeq2 (87). Box plots were generated using the ggplot2 package (v3.3.2 https://ggplot2.tidyverse.org/). For the Kwong et al. dataset (31), RNA-seq data were collected from European Genome-phenome Archive with accession EGAS000010000992. Tumor samples were limited to patients treated with dabrafenib (BRAFi) and trametinib (MEKi). Log-transformed NR2F1 expression levels were modeled in linear mixed effects (LME) model with the fixed effects of paper source of the data (Kwong *vs.* Song/Hugo/Lo) and time (pre-BRAFi + MEKi *vs.* on BRAFi + MEKi) and random effects of patient to adjust for correlation between two paired observations per patient. The final model included

only paper source of the data and time as predictors of NR2F1 expression levels. The paired difference between pre-BRAFi + MEKi and on BRAFi + MEKi was also analyzed separately for each dataset using the Wilcoxon two-sided two-sample test. The analysis was performed in R.

Xenograft and cell line RNA-seq datasets: For the Rambow et al. dataset (13), raw scRNA-seq counts data from BRAFi + MEKi treated cutaneous melanoma xenografts resected at different response states were downloaded from the Gene Expression Omnibus GEO database, accession GSE116237. Data were analyzed using the Seurat package (94). Expression levels of NR2F1 were explored based on the MRD cell type calls in Rambow et al. (13). For the Tsoi et al. dataset (34), RNA-seq data were gathered from GEO, accession GSE80829. Melanoma cell state data were gathered from Tsoi et al. (34). The independent-samples Kruskal Wallis Test was performed using the PMCMRplus package (v1.4.1 https://CRAN.R-project.org/package=PMCMRplus). Pairwise comparisons were calculated using Dunn's all-pairs test. Adjusted p-values were calculated using the Bonferroni method. Box plots were generated using the ggplot2 package (v3.1.0 https://ggplot2.tidyverse.org/). Data analyses were performed using R and RStudio (http://www.posit.co/).

Statistical analyses: For *in vitro* studies, data were expressed as mean ± standard deviation (SD) and statistically analyzed using Student's t-test (two-tailed, unpaired, and assuming unequal variance) with level of significance at $p<0.05$. Means and SD were calculated using at least three biological replicates (n=3). Significant differences among control and treated groups are indicated as *$p<0.05$, **$p<0.01$, and ***$p<0.001$. For *in vivo* studies, survival curves and curves showing the percentage (%) of tumor-free mice were analyzed using a Log-rank (Mantel-Cox) test. A p-value of <0.05 was considered statistically significant. Significance is denoted by *$p<0.05$, **$p<0.01$, ***$p<0.001$. All replicates for *in vitro* data are derived from independent experiments. No statistical method was used to predetermine sample size. No data were excluded from the analyses.

Experiments using cultured cells and mice were randomized. For detecting protein levels inside the cells and interactions of proteins, Western blot was conducted and repeated twice to confirm the results.

For the *in vivo* rapamycin regrowth experiment (Figures 5D and E), the tumor volume measures for each animal were interpolated using the smooth cubic splines, and resulting splines were used to approximate the time to regrow for each tumor (time to 100 mm^3). For tumors that did not regrow to 100 mm^3, the last day of observation was used as the time of censoring. The time to regrow was compared between treatment groups (RAPA vs. control) using the log-rank test. For mice with tumors that regrow to 100 mm^3, the exponential regrowth rates were estimated for each animal by modeling log-transformed tumor volumes in a linear mixed effects (LME) model with the fixed effects of day, treatment group, and interaction between day and treatment group. The model included random effects of animal in intercept and day to allow for animal-specific growth trajectories. The model was based on tumor volumes measure after tumors reached post-treatment nadir and regrow to at least 35 mm^3.

Study approval: All xenograft experiments were reviewed and approved by the Institutional Animal Care and Use Committee (IACUC protocol #01052) and performed in a facility at Thomas Jefferson University accredited by the Association for the Assessment and Accreditation of Laboratory Animal Care (AAALAC).

Data Availability

All data generated in this study are available within the article and the supplementary data files. All supporting data values are available in the supporting data value XLS file. All raw western blots are also included in the raw western blot document. All RNA-seq data are accessible on NCBI's GEO and can be accessed through GSE228600. All code used in this study is available at: https://github.com/AplinLabBioinformatics

ACKNOWLEDGEMENTS

This work is supported by grants from National Institutes of Health (NIH) R01 CA160495 to A.E.A. and CA253977 to A.E.A. and J.A.G. In addition, the study was supported by Dr. Miriam and Sheldon G. Adelson Medical Research Foundation awards to A.E.A. and M.A.D. The Sidney Kimmel Comprehensive Cancer Center Flow Cytometry, Translational Pathology, BioImaging, and Cancer Genomics Shared Resource facilities are supported by NIH/National Cancer Institute Support Grant, P30 CA056036. We are grateful to Plexxikon Inc. for kindly providing PLX4720 and PD0325901 for *in vivo* experiments. We thank the Functional Proteomics Core Facility at The University of Texas, MD Anderson Cancer for performing RPPA studies. At Thomas Jefferson University, we thank Dr. Maria Yolanda Covarrubias for her help with confocal microscopy; Mrs. Pamela Walter, Ms. Kristine Luo, and Ms. Signe Caksa for reviewing the manuscript; and Dr. Lei Yu and Mr. Amir Yarmahmoodi for cell sorting. We would like to thank Dr. Lauren Langbein, a scientific writer for the Sidney Kimmel Comprehensive Cancer Center, for assistance in finalizing the manuscript.

LEAD CONTACT AND MATERIALS AVAILABILITY

All unique/stable reagents generated in this study are available from the lead contact with a completed Materials Transfer Agreement. All requests should be directed to Andrew E. Aplin (Andrew.Aplin@jefferson.edu).

AUTHOR CONTRIBUTIONS

M.T. conceived the study, designed research, performed most experiments, analyzed the data, and wrote the manuscript. **T.J.P.** performed and provided guidance on computational analyses and related figures present in the manuscript. **C.D.S.** performed *in vitro* CRT experiments and *in vivo* BRAFi + MEKi + rapamycin MRD experiments. **R.O.S.** performed *in vitro* cell death experiments. **J.H.** performed computational analyses. **M.E.F.** helped design and perform all

683 experiments regarding shRNA NR2F1 in young and aged tumor microenvironments *in vitro* and
684 *in vivo*. **Y.C.** helped with shRNA NR2F1 in young and old mice models. **J.L.F.T.** provided NR2F1-
685 overexpressing cell lines, helped design and gave feedback regarding cell colony, spheroid, and
686 xenograft experiments. **R.M.** provided technical support regarding immunofluorescence for
687 NR2F1 in residual tumors on BRAFi + MEKi. **W.C.** provided technical support and helped with *in*
688 *vivo* experiments. **I.C.** performed statistical analysis for publicly available patient sample datasets
689 and *in vivo* rapamycin experiments. **S.R.** helped with *in vivo* experiments. **V.C.** helped with
690 gavage in mouse experiments. **N.H.** provided RNA-seq analysis. **M.A.D.** provided RPPA analysis.
691 **J.V.** gave feedback regarding targeting phospho-S6. **A.W.** provided young and aged mice for *in*
692 *vivo* experiments and gave feedback regarding experimental design. **D.A.E.** helped with
693 analyzing the data, prepared figures, and helped with writing the revised manuscript. **C.C.** helped
694 in the conception of the project, analyzing the data, reviewed the manuscript and gave feedback
695 regarding the manuscript layout. **J.A.G.** provided technical support regarding
696 immunofluorescence for NR2F1 in residual tumors on BRAFi + MEKi, reviewed the manuscript,
697 and gave feedback regarding the manuscript concept. **A.E.A.** conceived of the study, designed
698 the research, and wrote the manuscript.
699

FIGURE LEGENDS

Figure 1. NR2F1 is highly expressed in patient melanoma lesions on BRAF and MEK inhibitors therapy. (A) Normalized expression of NR2F1 for baseline or pre-treatment (Pre) and early during treatment (On) tumor samples from patients who received BRAF inhibitor and MEK inhibitor (BRAFi + MEKi) combination therapy in datasets from Song/Hugo/Lo et al., 2017 (33) (left panel) and Kwong et al., 2015 (31) (right panel). **(B)** Boxplot of NR2F1 RNA-seq gene expression data for melanoma cell lines categorized across cell states. Dataset from Tsoi et al. (34). **(C)** Violin plot of NR2F1 expression levels by cell state in scRNA-seq dataset of patient-derived xenograft (PDX) melanomas following BRAFi + MEKi treatment from Rambow et al. (13). Cell types present during MRD are shown. NCSC, Neural Crest Stem Cell; SMC, “Starved”-like Melanoma Cell. **(D)** Tumor volume in mice bearing 1205Lu-tdTomato-labeled xenografts following continuous BRAFi + MEKi (PLX4720 200 ppm + PD0325901 7 ppm) for three weeks. **(E)** Representative detection of tdTomato fluorescence representing tumor size in xenografts after three weeks on BRAFi + MEKi therapy (left panel); and mean nuclear intensity of NR2F1 protein expression in 1205Lu-tdTomato cells by immunofluorescence of tumor xenografts compared to no-drug treatment control group (right panel). T-Test.

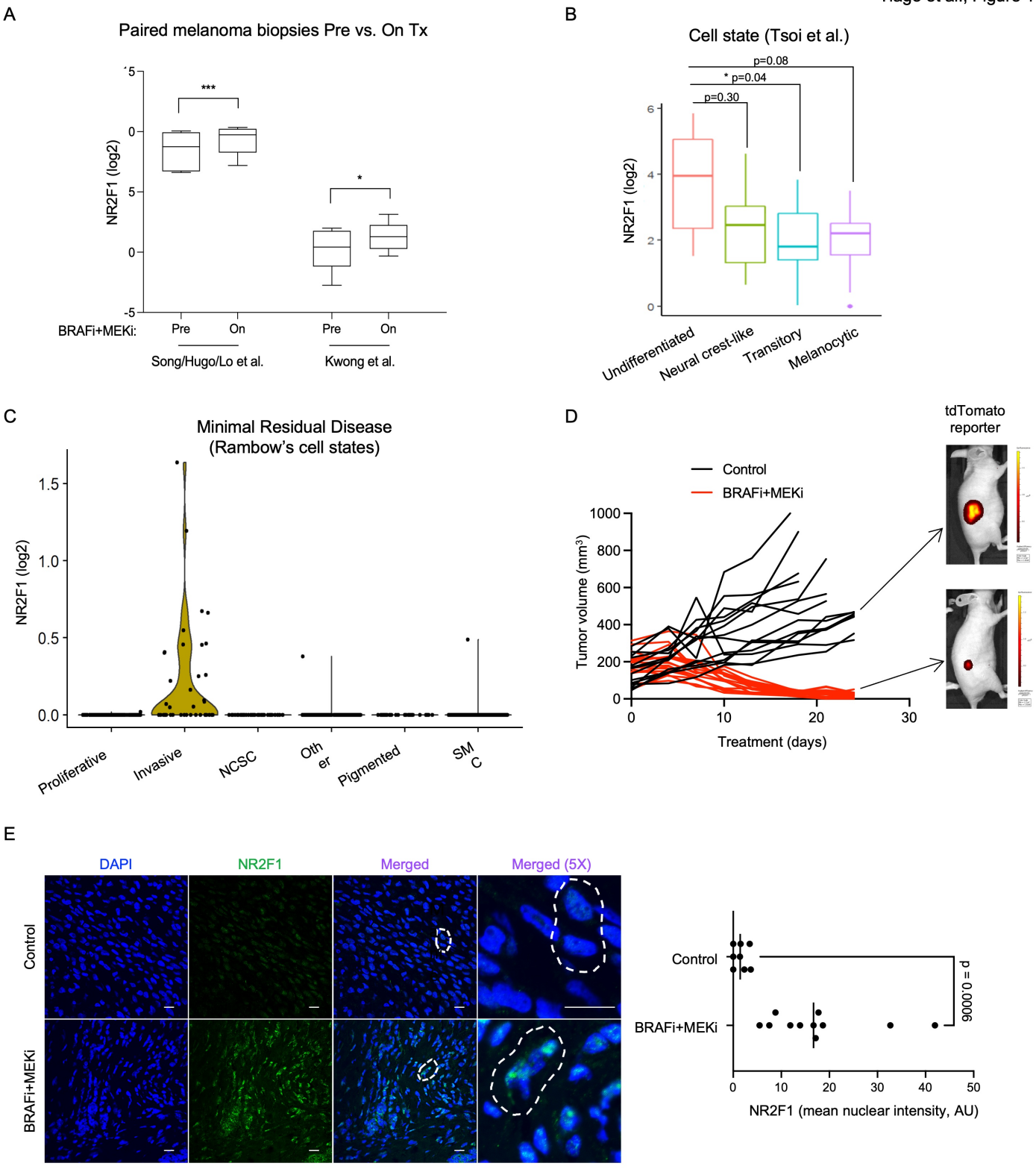
A
Paired melanoma biopsies Pre vs. On Tx
NR2F1 (log2)
***
*
BRAFi+MEKi:
Pre
On
Pre
On
Song/Hugo/Lo et al.
Kwong et al.
B
Cell state (Tsoi et al.)
p=0.08
* p=0.04
p=0.30
NR2F1 (log2)
Undifferentiated
Neural crest-like
Transitory
Melanocytic
C
Minimal Residual Disease
(Rambow's cell states)
NR2F1 (log2)
Proliferative
Invasive
NCSC
Other
Pigmented
SMC
D
tdTomato
reporter
Control
BRAFi+MEKi
Tumor volume (mm³)
Treatment (days)
E
DAPI
NR2F1
Merged
Merged (5X)
Control
BRAFi+MEKi
Control
BRAFi+MEKi
p = 0.0006
NR2F1 (mean nuclear intensity, AU)

Figure 2. NR2F1 overexpression minimizes tumor inhibition effects by BRAF inhibitor and MEK inhibitor therapy. (A) NR2F1 protein levels in human *BRAF*-mutant melanoma cell lines expressing doxycycline inducible NR2F1, 1205LuTR-NR2F1, WM793TR-NR2F1, and A375TR-NR2F1, after 72 hours of treatment using BRAFi + MEKi + DOX (PLX4720 1 μmol/L + PD0325901 35 nmol/L + doxycycline 100 ng/mL). **(B)** Colony assay for cell lines overexpressing DOX-inducible NR2F1 after one week of treatment using BRAFi + MEKi + DOX. Magnification: 20X. **(C)** S-phase cell cycle detection arrest by EdU staining for the *BRAF*-mutant human melanoma cell lines listed above after 72 hours of treatment using BRAFi + MEKi + DOX. Tukey's test (**p*<0.05, ****p*<0.001). **(D)** Propidium iodide (PI) uptake over cell confluence in the *BRAF*-mutant human melanoma cell lines listed above after 72 hours of treatment using BRAFi + MEKi + DOX as determined by IncuCyte analysis. Tukey's test (**p*<0.05, ***p*<0.01). **(E)** Representative figures of 3D tumor spheroids for human *BRAF*-mutant melanoma cell lines, 1205LuTR-NR2F1, WM793TR-NR2F1, and A375TR-NR2F1, after 72 hours of treatment using BRAFi + MEKi + DOX (PLX4720 1 μmol/L + PD0325901 35 nmol/L + doxycycline 100 ng/mL). 3D tumor spheroids were stained with calcein-AM (7 μmol/L) for cell viability evaluation. Scale bars: 100 μm. Magnification: 200X. **(F)** Scheme of co-culture of tdTomato-cells overexpressing DOX-inducible NR2F1 wild-type (95) and GFP-cells overexpressing a DOX-inducible dominant-negative form of NR2F1 (39) harboring a C141S point mutation within its DNA-binding domain (C141S). Cells were mixed at the ratio of 1:1, and then co-cultured for 72 hours in the presence or absence of BRAFi + MEKi + DOX (PLX4720 1 μmol/L + PD0325901 35 nmol/L + doxycycline 100 ng/mL). Co-cultures from **(F)** were collected and analyzed by FACS for tdTomato and GFP positivity; **(G)** the percentage of tdTomato and GFP positivity was compared to DMSO.

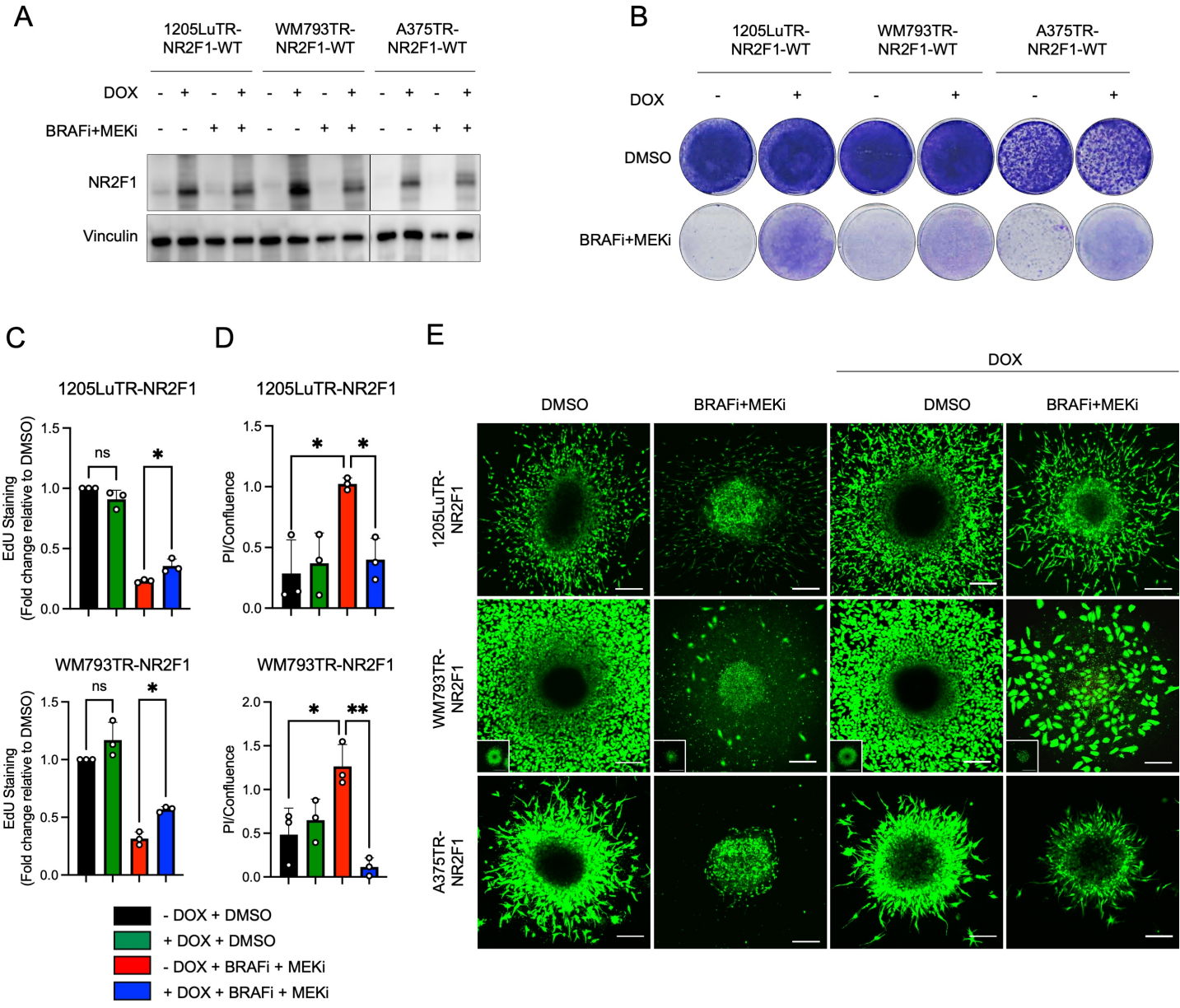
A
1205LuTR-NR2F1-WT
WM793TR-NR2F1-WT
A375TR-NR2F1-WT
DOX
BRAFi+MEKi
NR2F1
Vinculin
B
DMSO
C
1205LuTR-NR2F1
EdU Staining (Fold change relative to DMSO)
ns
WM793TR-NR2F1
D
PI/Confluence
E
DOX
1205LuTR-NR2F1
WM793TR-NR2F1
A375TR-NR2F1
- DOX + DMSO
+ DOX + DMSO
- DOX + BRAFi + MEKi
+ DOX + BRAFi + MEKi
F
TetR-tdTomato-NR2F1-WT
TetR-GFP-NR2F1-C141S
Co-culture (1:1)
BRAFi+MEKi
DOX
Flow Cytometry for tdTomato- and GFP-cells
G
1205LuTR
WM793TR
Cells (%)
NR2F1-WT
NR2F1-C141S

Figure 3. NR2F1 overexpression promotes tumor relapse following BRAF and MEK inhibitors therapy. (A) IncuCyte live-cell analysis for DOX-inducible cells overexpressing NR2F1 after four weeks of treatment using BRAFi + MEKi + DOX (PLX4720 1 μmol/L + PD0325901 35 nmol/L + doxycycline 100 ng/mL). Data was analyzed for percent cell confluency on the plate. **(B)** NR2F1 protein levels for the DOX-inducible NR2F1-expressing cell line, 1205Lu-E2F-tdTomato(tdTW)-TR-NR2F1, after 72 hours of treatment using BRAFi + MEKi + DOX. **(C)** *In vivo* tumor growth curves and **(D)** survival of 1205Lu xenografts with DOX-inducible NR2F1 expression following BRAFi + MEKi (PLX4720 200 ppm + PD0325901 7 ppm + doxycycline 25 mg/mL) treatment. Kaplan-Meier analysis (***$p<0.001$).

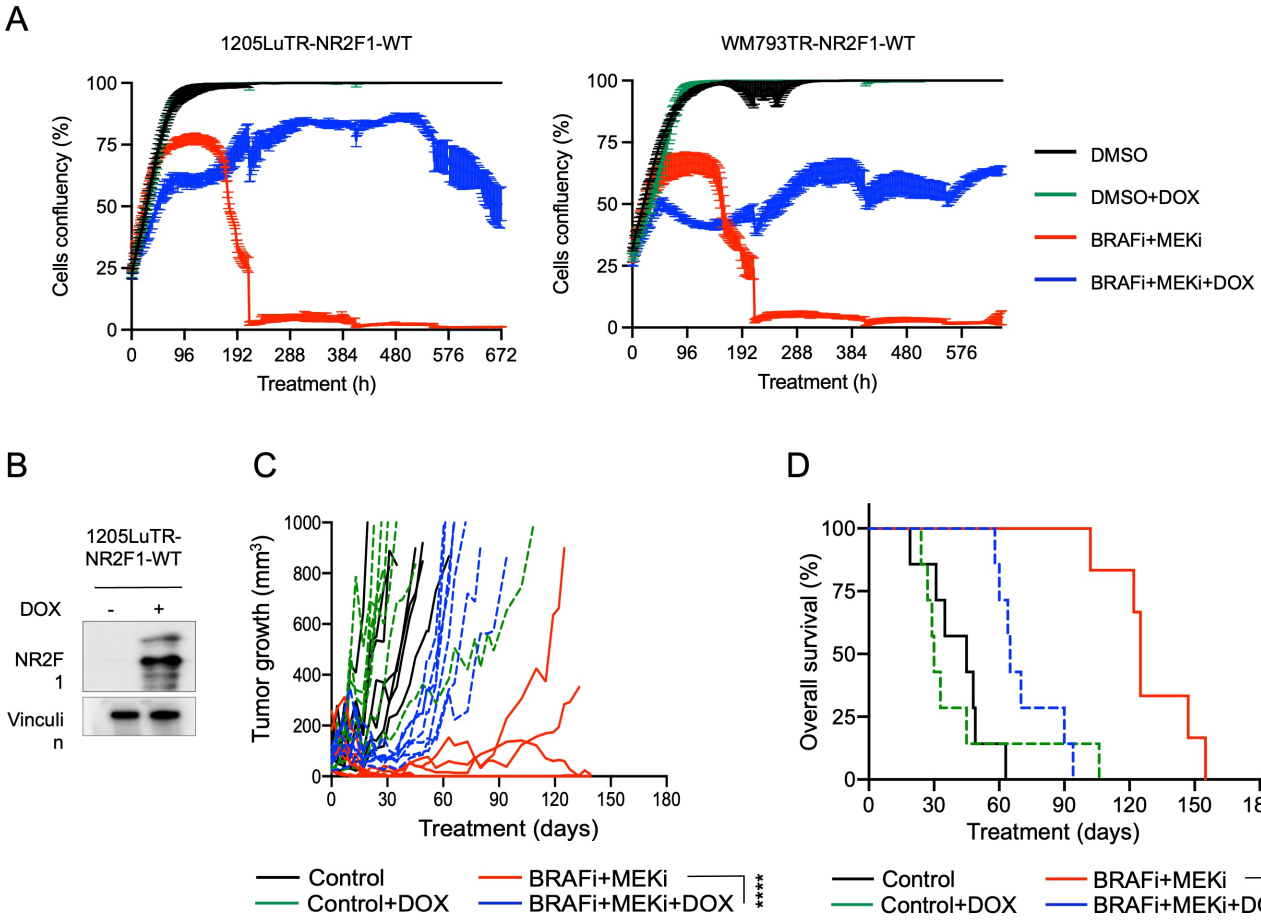
A
1205LuTR-NR2F1-WT
WM793TR-NR2F1-WT
Cells confluency (%)
Treatment (h)
DMSO
DMSO+DOX
BRAFi+MEKi
BRAFi+MEKi+DOX
B
1205LuTR-NR2F1-WT
DOX
NR2F1
Vinculin
C
Tumor growth (mm3)
Treatment (days)
Control
Control+DOX
BRAFi+MEKi
BRAFi+MEKi+DOX
****
D
Overall survival (%)
Treatment (days)
***

Figure 4. NR2F1 overexpression upregulates cell proliferation and mTORC1 signaling following BRAF and MEK inhibitors therapy. (A) Heatmap showing GSEA normalized enrichment scores (NES) for the hallmark gene sets collection comparing NR2F1 expression to no DOX after 72 hours of treatment using BRAFi + MEKi + DOX (PLX4720 1 µmol/L + PD0325901 35 nmol/L + doxycycline 100 ng/mL) in 1205LuTR-NR2F1, WM793TR-NR2F1, and A375TR-NR2F1 cell samples. NES values are displayed for enriched gene sets, using a Benjamini-Hochberg False Discovery Rate (BHFDR) cutoff 0.05. **(B)** GSEA hallmark enrichment plots for mTORC1 response for the same cells and drug treatments above. **(C)** Reverse phase protein array (RPPA) analysis for the *BRAF*-mutant human melanoma cell lines, 1205LuTR-NR2F1, WM793TR-NR2F1, and A375TR-NR2F1, after 72 hours of treatment using BRAFi + MEKi + DOX. Median centered, log2-transformed group average RPPA expression data for targets with at least 25% change when comparing NR2F1 expression to no DOX after 72 hours of treatment. **(D)** Representative western blot for RPPA-identified proteins in **(C)** after treatment with BRAFi + MEKi for 72 hours (n=2-3); quantification of band densitometry (phosphorylated proteins compared to total protein [e.g., RB (pS780):RB] normalized to no BRAFi + MEKi + no DOX conditions) is displayed under each band. Please note that the NR2F1 blot is the same here and in Supplemental Figure S4A. **(E)** A heatmap showing hierarchical clustering of commonly enriched genes in mTORC1 GSEA results for all three cell line comparisons of BRAFi + MEKi + DOX. **(F)** MACS2 fold enrichment values are displayed for genes with NR2F1 ChIP-seq binding in their promoter region (n=17, each ChIP-seq experiment is represented by a dot) from the genes in **(E)**.

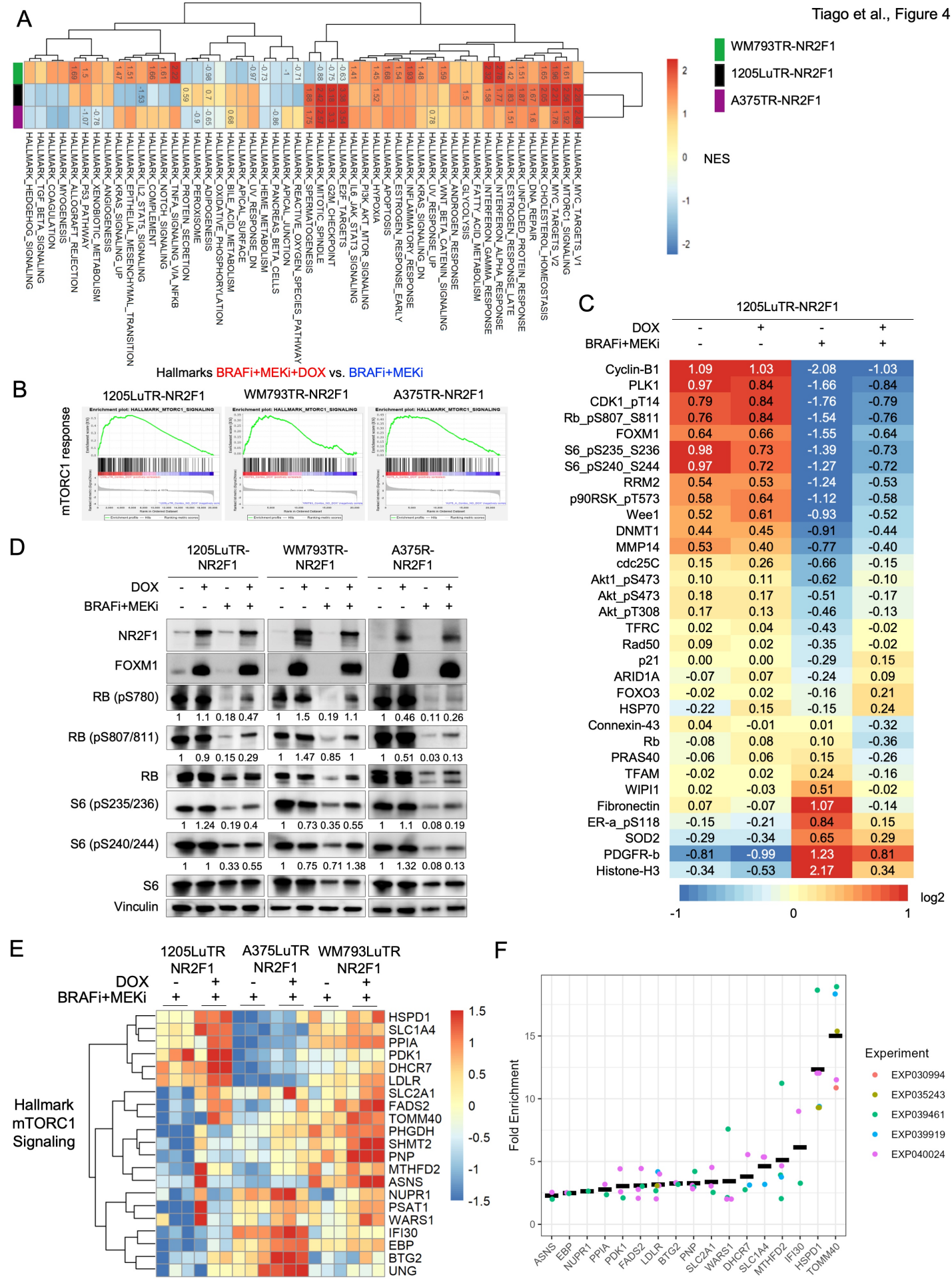
A
WM793TR-NR2F1
1205LuTR-NR2F1
A375TR-NR2F1
NES
Hallmarks BRAFi+MEKi+DOX vs. BRAFi+MEKi
B
1205LuTR-NR2F1
WM793TR-NR2F1
A375TR-NR2F1
mTORC1 response
C
1205LuTR-NR2F1
DOX
BRAFi+MEKi
Cyclin-B1 1.09 1.03 -2.08 -1.03
PLK1 0.97 0.84 -1.66 -0.84
CDK1_pT14 0.79 0.84 -1.76 -0.79
Rb_pS807_S811 0.76 0.84 -1.54 -0.76
FOXM1 0.64 0.66 -1.55 -0.64
S6_pS235_S236 0.98 0.73 -1.39 -0.73
S6_pS240_S244 0.97 0.72 -1.27 -0.72
RRM2 0.54 0.53 -1.24 -0.53
p90RSK_pT573 0.58 0.64 -1.12 -0.58
Wee1 0.52 0.61 -0.93 -0.52
DNMT1 0.44 0.45 -0.91 -0.44
MMP14 0.53 0.40 -0.77 -0.40
cdc25C 0.15 0.26 -0.66 -0.15
Akt1_pS473 0.10 0.11 -0.62 -0.10
Akt_pS473 0.18 0.17 -0.51 -0.17
Akt_pT308 0.17 0.13 -0.46 -0.13
TFRC 0.02 0.04 -0.43 -0.02
Rad50 0.09 0.02 -0.35 -0.02
p21 0.00 0.00 -0.29 0.15
ARID1A -0.07 0.07 -0.24 0.09
FOXO3 -0.02 0.02 -0.16 0.21
HSP70 -0.22 0.15 -0.15 0.24
Connexin-43 0.04 -0.01 0.01 -0.32
Rb -0.08 0.08 0.10 -0.36
PRAS40 -0.06 0.06 0.15 -0.26
TFAM -0.02 0.02 0.24 -0.16
WIPI1 0.02 -0.03 0.51 -0.02
Fibronectin 0.07 -0.07 1.07 -0.14
ER-a_pS118 -0.15 -0.21 0.84 0.15
SOD2 -0.29 -0.34 0.65 0.29
PDGFR-b -0.81 -0.99 1.23 0.81
Histone-H3 -0.34 -0.53 2.17 0.34
log2
D
1205LuTR-NR2F1
WM793TR-NR2F1
A375R-NR2F1
DOX
BRAFi+MEKi
NR2F1
FOXM1
RB (pS780)
1 1.1 0.18 0.47 1 1.5 0.19 1.1 1 0.46 0.11 0.26
RB (pS807/811)
1 0.9 0.15 0.29 1 1.47 0.85 1 1 0.51 0.03 0.13
RB
S6 (pS235/236)
1 1.24 0.19 0.4 1 0.73 0.35 0.55 1 1.1 0.08 0.19
S6 (pS240/244)
1 1 0.33 0.55 1 0.75 0.71 1.38 1 1.32 0.08 0.13
S6
Vinculin
E
1205LuTR NR2F1
A375LuTR NR2F1
WM793LuTR NR2F1
DOX
BRAFi+MEKi
Hallmark mTORC1 Signaling
HSPD1
SLC1A4
PPIA
PDK1
DHCR7
LDLR
SLC2A1
FADS2
TOMM40
PHGDH
SHMT2
PNP
MTHFD2
ASNS
NUPR1
PSAT1
WARS1
IFI30
EBP
BTG2
UNG
F
Fold Enrichment
Experiment
EXP030994
EXP035243
EXP039461
EXP039919
EXP040024
ASNS EBP NUPR1 PPIA PDK1 FADS2 LDLR BTG2 PNP SLC2A1 WARS1 DHCR7 SLC1A4 MTHFD2 IFI30 HSPD1 TOMM40

Figure 5. Rapamycin targets NR2F1-overexpressing drug-tolerant cells and delays tumor growth. (A) Colony assay for cell lines overexpressing DOX-inducible NR2F1 after one week of treatment using BRAFi + MEKi + mTORC1i (either AZD2014, 1 μmol/L, or rapamycin, 1 μmol/L). Magnification: 20X. **(B)** IncuCyte live-cell analysis for DOX-inducible cells overexpressing NR2F1 after four weeks of treatment using BRAFi + MEKi + DOX. Cell growth was analyzed for percent cell confluency on the plate (representative of three independent experiments). **(C)** Expression of NR2F1 in MRD state following BRAFi + MEKi + rapamycin (4 mg/kg) *in vivo*. Mice bearing 1205Lu-tdTomato-labeled xenografts following continuous BRAFi + MEKi chow (PLX4720 200 ppm + PD0325901 7 ppm) for three weeks, then either control chow + vehicle (Control), control chow + rapamycin 4 mg/kg (rapamycin), BRAFi + MEKi chow + vehicle (BRAFi+MEKi), or BRAFi + MEKi chow + rapamycin (BRAFi + MEKi + rapamycin) for one week (left panel); and mean nuclear intensity of NR2F1 protein expression in MRD tumor xenografts by immunofluorescence compared to control (right panel). Two way anova. **(D)** Mice bearing 1205Lu-tdTomato-labeled xenografts following continuous BRAFi + MEKi chow (PLX4720 200 ppm + PD0325901 7 ppm) until tumors entered a state of MRD for several weeks (day 52 post-BRAFi + MEKi), then either continuous BRAFi + MEKi chow + vehicle (BRAFi + MEKi), or continuous BRAFi + MEKi chow + 4 mg/kg rapamycin twice per week (BRAFi + MEKi + rapamycin) began for the duration of the experiment (treatment start indicated with dotted line on x-axis). Shown is the tumor growth of treated mice. An X on a tracing denotes an animal that was sacrificed due to non-experimental reasons. **E)** Table displaying the estimated exponential regrowth rates and their difference in tumors that regrow to 100 mm^3 from the BRAFi + MEKi + rapamycin and BRAFi + MEKi + control groups from panel D. Statistical analysis is described in the methods.

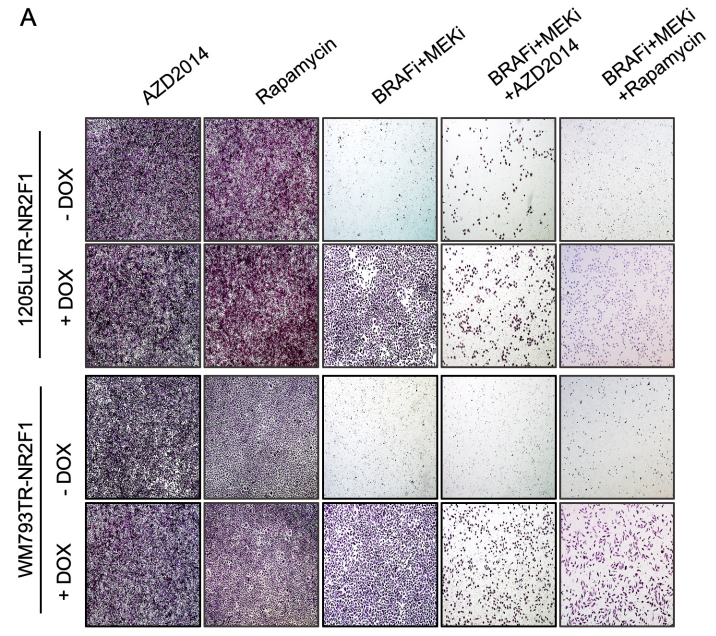

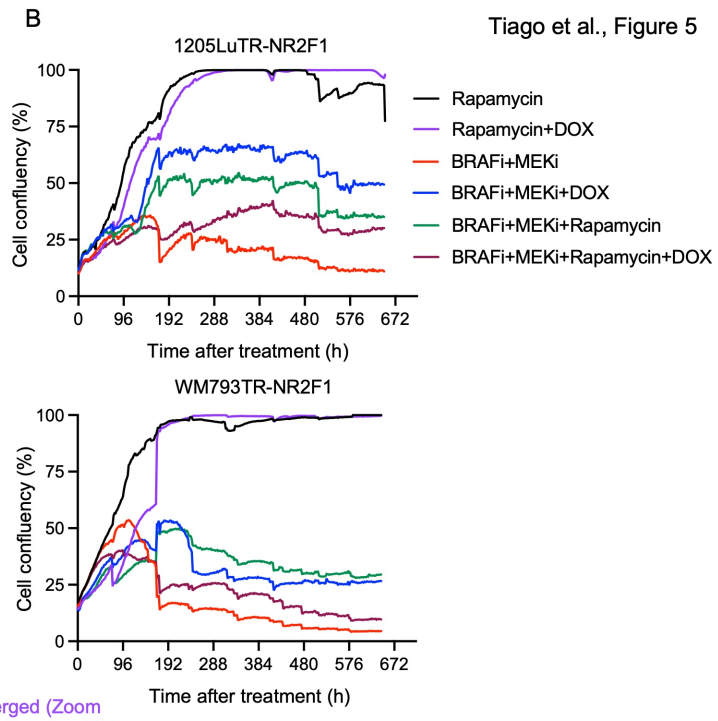

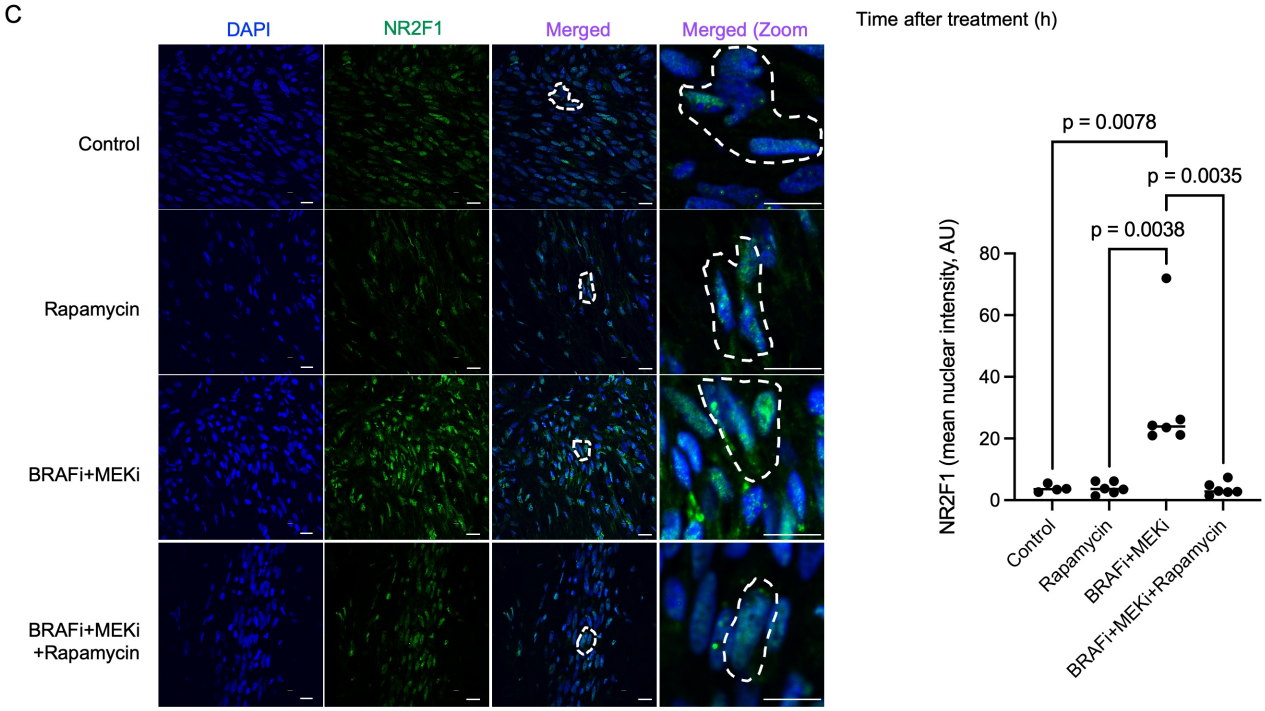

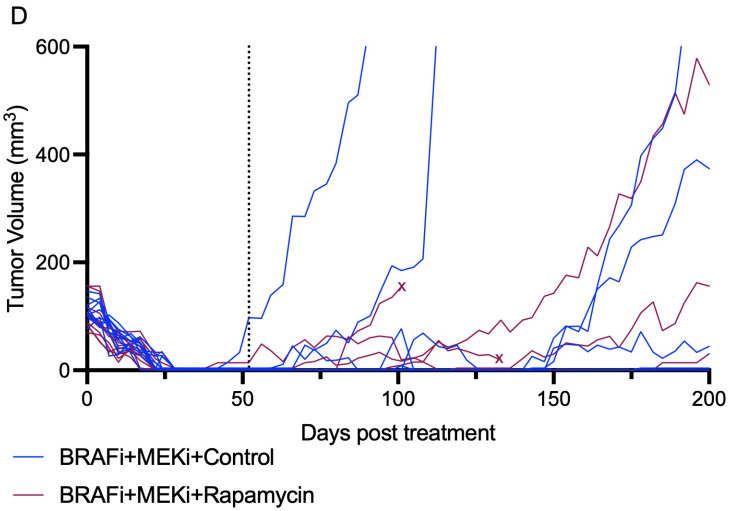

E

Estimated Mean Exponential Growth Rate after tumor onset

Tx group	Mean Exponential Growth Rate	Lower 95% CL	Upper 95% CL	P-value
BRAFi+MEKI+Control	5.20%	4.40%	6.10%	<0.001
BRAFi+MEKI+Rapamycin	3.00%	2.10%	3.90%	<0.001

Estimated Difference in Exponential Growth Rate after tumor onset

Tx group	Mean Diff in Exponential Growth Rate	Lower 95% CL	Upper 95% CL	P-value
Rapamycin vs. Control	-2.10%	-3.30%	-1.00%	0.0005

Figure 6. NR2F1 is overexpressed in aged *BRAF*-mutant melanoma models. (A) NR2F1 protein expression in cells cultured in conditioned media derived from fibroblasts isolated from young (<35 years old) and aged individuals (>55 years old) and **(B)** YUMM1.7 tumor allografts from young *vs.* aged mice stained with NR2F1 and quantified for % of positive nuclei using ImageJ. **(C)** NR2F1 inhibition by lentiviral DOX-inducible expression of shRNA targeting NR2F1 (tumors in both groups were >500 mm^3). **(D)** *In vivo* tumor growth curves (**p=0.004127, comparing BRAFi + MEKi alone to BRAFi + MEKi + DOX) and **(E)** survival of YUMM1.7 allografts with DOX-inducible shRNA targeting NR2F1 following BRAFi + MEKi + DOX (PLX4720 200 ppm + PD0325901 7 ppm + doxycycline 25 mg/mL) treatment. Kaplan-Meier analysis (**p=0.004).

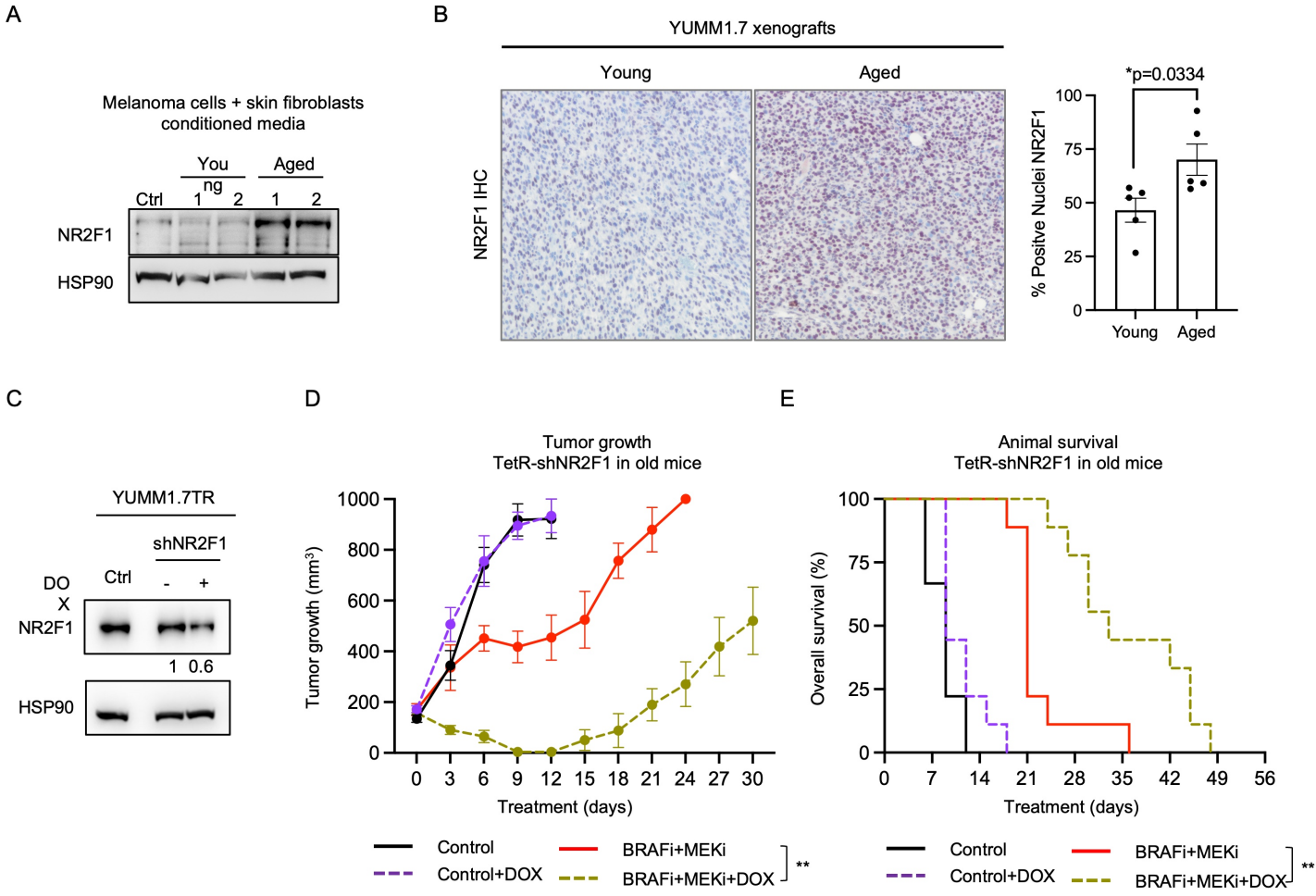
A
Melanoma cells + skin fibroblasts conditioned media
You
Aged
ng
Ctrl
1
2
1
2
NR2F1
HSP90
B
YUMM1.7 xenografts
Young
Aged
NR2F1 IHC
*p=0.0334
% Positive Nuclei NR2F1
100
75
50
25
0
Young
Aged
C
YUMM1.7TR
shNR2F1
DO
X
Ctrl
-
+
NR2F1
1
0.6
HSP90
D
Tumor growth
TetR-shNR2F1 in old mice
Tumor growth (mm3)
1000
800
600
400
200
0
0
3
6
9
12
15
18
21
24
27
30
Treatment (days)
Control
Control+DOX
BRAFi+MEKi
BRAFi+MEKi+DOX
**
E
Animal survival
TetR-shNR2F1 in old mice
Overall survival (%)
100
75
50
25
0
0
7
14
21
28
35
42
49
56
Treatment (days)
Control
Control+DOX
BRAFi+MEKi
BRAFi+MEKi+DOX
**

Figure 7. Graphical abstract of the role of NR2F1 in the persistence of minimal residual disease in melanoma. BRAFi + MEKi-tolerant persister cells express NR2F1 during MRD. NR2F1-overexpressing cells show upregulation of the mTORC1 pathway. Knockdown of NR2F1 or mTORC1 pathway inhibition delays tumor recurrence in cutaneous melanoma.

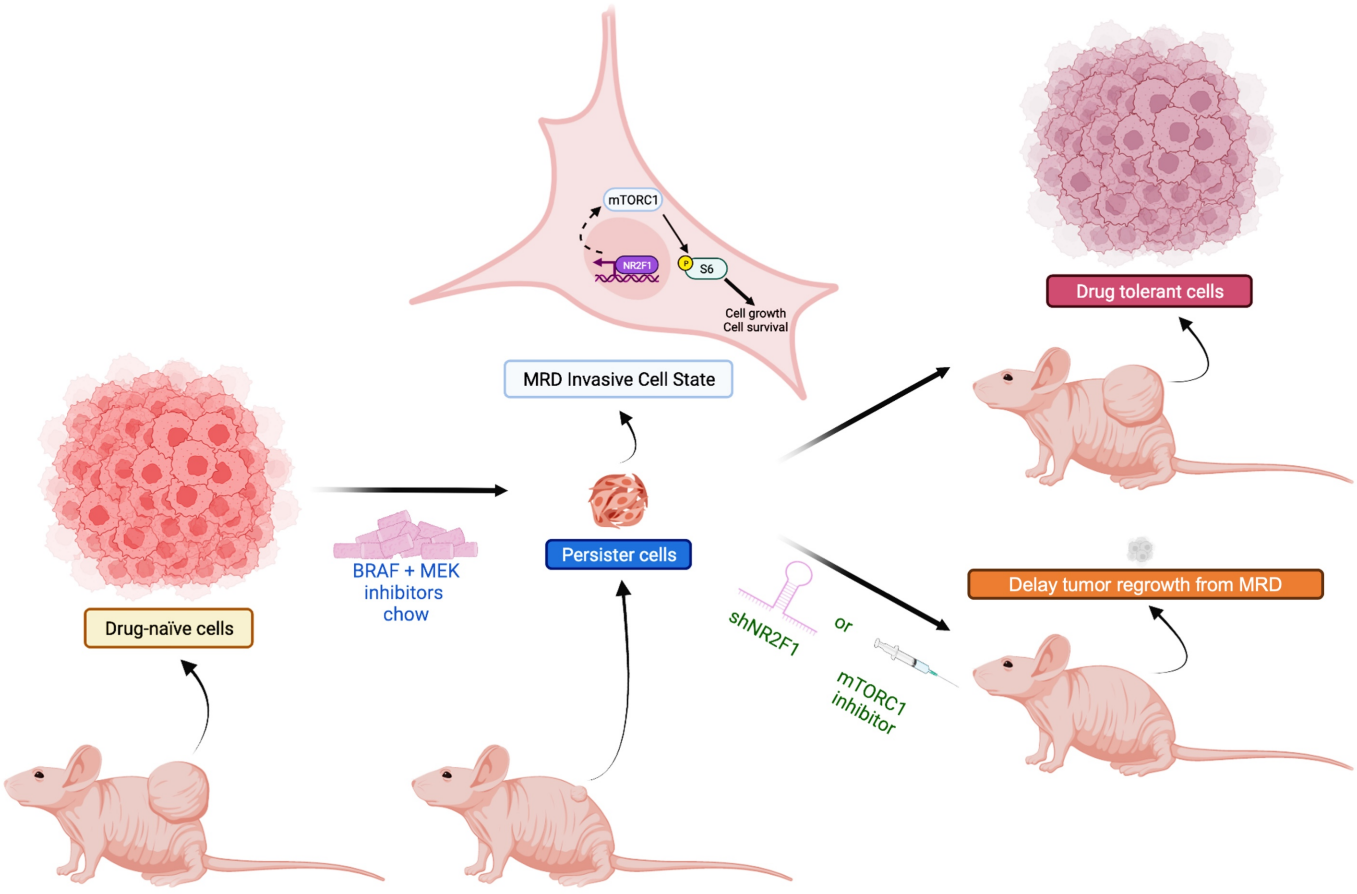
mTORC1
NR2F1
P
S6
Cell growth
Cell survival
MRD Invasive Cell State
Drug tolerant cells
Drug-naïve cells
BRAF + MEK
inhibitors
chow
Persister cells
shNR2F1
or
mTORC1
inhibitor
Delay tumor regrowth from MRD

REFERENCES

1. Fattore L, et al. Cancer stem cells and the slow cycling phenotype: how to cut the gordian knot driving resistance to therapy in melanoma. *Cancers (Basel).* 2020;12(11):3368.
2. Michielin O, et al. Evolving impact of long-term survival results on metastatic melanoma treatment. *J Immunother Cancer.* 2020;8(2):e000948.
3. Bhave P, et al. Melanoma recurrence patterns and management after adjuvant targeted therapy: a multicentre analysis. *Br J Cancer.* 2021;124(3):574-80.
4. Savoia P, et al. Clinical implications of acquired BRAF inhibitors resistance in melanoma. *Int J Mol Sci.* 2020;21(24):9730.
5. Fane M, and Weeraratna AT. How the ageing microenvironment influences tumour progression. *Nat Rev Cancer.* 2020;20(2):89-106.
6. Bragado P, et al. Microenvironments dictating tumor cell dormancy. *Recent Results Cancer Res.* 2012;195:25-39.
7. Kaur A, et al. sFRP2 in the aged microenvironment drives melanoma metastasis and therapy resistance. *Nature.* 2016;532(7598):250-4.
8. Alicea GM, et al. Changes in aged fibroblast lipid metabolism induce age-dependent melanoma cell resistance to targeted therapy via the fatty acid transporter FATP2. *Cancer Discov.* 2020;10(9):1282-95.
9. Fane ME, et al. Stromal changes in the aged lung induce an emergence from melanoma dormancy. *Nature.* 2022;606(7913):396-405.
10. Chhabra Y, et al. Sex-dependent effects in the aged melanoma tumor microenvironment influence invasion and resistance to targeted therapy. *Cell.* 2024;187(21):6016-34.e25.
11. Swayden M, et al. Tolerant/persister cancer cells and the path to resistance to targeted therapy. *Cells.* 2020;9(12):2601.
12. Atkins MB, et al. The state of melanoma: emergent challenges and opportunities. *Clin Cancer Res.* 2021;27(10):2678-97.

838 13. Rambow F, et al. Towards minimal residual disease-directed therapy in melanoma. *Cell*.
839 2018;174(4):843-55.e19.
840 14. Bristot IJ, et al. Metabolic rewiring in melanoma drug-resistant cells. *Crit Rev Oncol*
841 *Hematol.* 2020;153(2020):102995.
842 15. Ahn A, et al. The slow cycling phenotype: a growing problem for treatment resistance in
843 melanoma. *Mol Cancer Ther.* 2017;16(6):1002-9.
844 16. Perego M, et al. A slow-cycling subpopulation of melanoma cells with highly invasive
845 properties. *Oncogene.* 2018;37(3):302-12.
846 17. Jahanban-Esfahlan R, et al. Tumor cell dormancy: threat or opportunity in the fight against
847 cancer. *Cancers (Basel).* 2019;11(8):1207.
848 18. Risson E, et al. The current paradigm and challenges ahead for the dormancy of
849 disseminated tumor cells. *Nat Cancer.* 2020;1(7):672-80.
850 19. Glasheen MQ, et al. Targeting up-regulated cIAP2 in SOX10-deficient drug tolerant
851 melanoma. *Mol Cancer Ther.* 2023;22(9):1087-99.
852 20. Zhang G, and Herlyn M. Linking SOX10 to a slow-growth resistance phenotype. *Cell Res.*
853 2014;24(8):906-7.
854 21. Uka R, et al. Temporal activation of WNT/beta-catenin signaling is sufficient to inhibit
855 SOX10 expression and block melanoma growth. *Oncogene.* 2020;39(20):4132-54.
856 22. Kemper K, et al. Phenotype switching: tumor cell plasticity as a resistance mechanism
857 and target for therapy. *Cancer Res.* 2014;74(21):5937-41.
858 23. Yeh AC, and Ramaswamy S. Mechanisms of cancer cell dormancy--another hallmark of
859 cancer? *Cancer Res.* 2015;75(23):5014-22.
860 24. Qin Y, et al. PERK mediates resistance to BRAF inhibition in melanoma with impaired
861 PTEN. *NPJ Precis Oncol.* 2021;5:68.
862 25. Capparelli C, et al. Targeting SOX10-deficient cells to reduce the dormant-invasive
863 phenotype state in melanoma. *Nat Commun.* 2022;13:1381.

26. Aguirre-Ghiso JA, et al. ERK(MAPK) activity as a determinant of tumor growth and dormancy; regulation by p38(SAPK). *Cancer Res.* 2003;63(7):1684-95.
27. Mikubo M, et al. Mechanism of drug tolerant persister cancer cells: the landscape and clinical implication for therapy. *J Thorac Oncol.* 2021;16(11):1798-809.
28. Sosa MS, et al. NR2F1 controls tumour cell dormancy via SOX9- and RARbeta-driven quiescence programmes. *Nat Commun.* 2015;6:6170.
29. Borgen E, et al. NR2F1 stratifies dormant disseminated tumor cells in breast cancer patients. *Breast Cancer Res.* 2018;20(1):120.
30. Rodriguez-Tirado C, et al. NR2F1 is a barrier to dissemination of early-stage breast cancer cells. *Cancer Res.* 2022;82(12):2313-26.
31. Kwong LN, et al. Co-clinical assessment identifies patterns of BRAF inhibitor resistance in melanoma. *J Clin Invest.* 2015;125(4):1459-70.
32. Kakavand H, et al. PD-L1 expression and immune escape in melanoma resistance to MAPK inhibitors. *Clin Cancer Res.* 2017;23(20):6054-61.
33. Song C, et al. Recurrent tumor cell-intrinsic and -extrinsic alterations during MAPKi-induced melanoma regression and early adaptation. *Cancer Discov.* 2018;7(11):1248-65.
34. Tsoi J, et al. Multi-stage differentiation defines melanoma subtypes with differential vulnerability to drug-induced iron-dependent oxidative stress. *Cancer Cell.* 2018;33(5):890-904 e5.
35. Sanchez IM, et al. In vivo ERK1/2 reporter predictively models response and resistance to combined BRAF and MEK inhibitors in melanoma. *Mol Cancer Ther.* 2019;18(9):1637-49.
36. Erkes DA, et al. Mutant BRAF and MEK Inhibitors Regulate the Tumor Immune Microenvironment via Pyroptosis. *Cancer Discov.* 2020;10(2):254-69.
37. Travnickova J, et al. Zebrafish MITF-low melanoma subtype models reveal transcriptional subclusters and MITF-independent residual disease. *Cancer Res.* 2019;79(22):5769-84.

38. Dilshat R, et al. MITF reprograms the extracellular matrix and focal adhesion in melanoma. *Elife.* 2021;10:e63093.
39. Adam F, et al. COUP-TFI (chicken ovalbumin upstream promoter-transcription factor I) regulates cell migration and axogenesis in differentiating P19 embryonal carcinoma cells. *Mol Endocrinol.* 2000;14(12):1918-33.
40. Eisenhauer EA, et al. New response evaluation criteria in solid tumours: revised RECIST guideline (version 1.1). *Eur J Cancer.* 2009;45(2):228-47.
41. Robert C, et al. Five-Year Outcomes with Dabrafenib plus Trametinib in Metastatic Melanoma. *N Engl J Med.* 2019;381(7):626-36.
42. Dummer R, et al. COLUMBUS 5-Year Update: A Randomized, Open-Label, Phase III Trial of Encorafenib Plus Binimetinib Versus Vemurafenib or Encorafenib in Patients With BRAF V600-Mutant Melanoma. *J Clin Oncol.* 2022;40(36):4178-88.
43. Ascierto PA, et al. Update on tolerability and overall survival in COLUMBUS: landmark analysis of a randomised phase 3 trial of encorafenib plus binimetinib vs vemurafenib or encorafenib in patients with BRAF V600-mutant melanoma. *Eur J Cancer.* 2020;126:33-44.
44. Kim RS, et al. Dormancy signatures and metastasis in estrogen receptor positive and negative breast cancer. *PLoS One.* 2012;7(4):e35569.
45. Zhang Y, et al. Model-based analysis of ChIP-Seq (MACS). *Genome Biol.* 2008;9(9):R137.
46. Yevshin I, et al. GTRD: a database on gene transcription regulation-2019 update. *Nucleic Acids Res.* 2019;47(D1):D100-D5.
47. Deng W, et al. Role and therapeutic potential of PI3K-mTOR signaling in de novo resistance to BRAF inhibition. *Pigment Cell Melanoma Res.* 2012;25(2):248-58.

914 48. Gopal YN, et al. Inhibition of mTORC1/2 overcomes resistance to MAPK pathway
915 inhibitors mediated by PGC1alpha and oxidative phosphorylation in melanoma. *Cancer*
916 *Res.* 2014;74(23):7037-47.
917 49. Guba M, et al. Rapamycin inhibits primary and metastatic tumor growth by
918 antiangiogenesis: involvement of vascular endothelial growth factor. *Nat Med.*
919 2002;8(2):128-35.
920 50. Day TA, et al. Inhibition of mTOR Signaling and Clinical Activity of Rapamycin in Head
921 and Neck Cancer in a Window of Opportunity Trial. *Clin Cancer Res.* 2019;25(4):1156-64.
922 51. Page AJ, et al. Increasing age is associated with worse prognostic factors and increased
923 distant recurrences despite fewer sentinel lymph node positives in melanoma. *Int J Surg*
924 *Oncol.* 2012;2012(456987):1-5.
925 52. Balch CM, et al. Age as a prognostic factor in patients with localized melanoma and
926 regional metastases. *Ann Surg Oncol.* 2013;20(12):3961-8.
927 53. Lo RS, and Shi H. Detecting mechanisms of acquired BRAF inhibitor resistance in
928 melanoma. *Methods Mol Biol.* 2014;1102:163-74.
929 54. De Angelis ML, et al. Stem cell plasticity and dormancy in the development of cancer
930 therapy resistance. *Front Oncol.* 2019;9(2019):626.
931 55. Cackowski FC, and Heath EI. Prostate cancer dormancy and recurrence. *Cancer Lett.*
932 2022;524(2022):103-8.
933 56. Shepherd TG, and Dick FA. Principles of dormancy evident in high-grade serous ovarian
934 cancer. *Cell Div.* 2022;17(1):2.
935 57. Ruth JR, et al. Cellular dormancy in minimal residual disease following targeted therapy.
936 *Breast Cancer Res.* 2021;23:63.
937 58. Perets R, et al. Genome-wide analysis of androgen receptor targets reveals COUP-TF1
938 as a novel player in human prostate cancer. *PLoS One.* 2012;7(10):e46467.

59. Hao Y, et al. Gene expression profiling reveals stromal genes expressed in common between Barrett's esophagus and adenocarcinoma. *Gastroenterology.* 2006;131(3):925-33.
60. Cheng PF, et al. Methylation-dependent SOX9 expression mediates invasion in human melanoma cells and is a negative prognostic factor in advanced melanoma. *Genome Biol.* 2015;16:42.
61. Yang X, et al. SOX9 is a dose-dependent metastatic fate determinant in melanoma. *J Exp Clin Cancer Res.* 2019;38(1):17.
62. Kruiswijk F, et al. Targeted inhibition of metastatic melanoma through interference with Pin1-FOXM1 signaling. *Oncogene.* 2016;35(17):2166-77.
63. Irvine M, et al. Oncogenic PI3K/AKT promotes the step-wise evolution of combination BRAF/MEK inhibitor resistance in melanoma. *Oncogenesis.* 2018;7(9):72.
64. Wang B, et al. Targeting mTOR signaling overcomes acquired resistance to combined BRAF and MEK inhibition in BRAF-mutant melanoma. *Oncogene.* 2021;40(37):5590-9.
65. Gao XL, et al. NR2F1 contributes to cancer cell dormancy, invasion and metastasis of salivary adenoid cystic carcinoma by activating CXCL12/CXCR4 pathway. *BMC Cancer.* 2019;19(1):743.
66. Borriello L, et al. Primary tumor associated macrophages activate programs of invasion and dormancy in disseminating tumor cells. *Nat Commun.* 2022;13:626.
67. Khalil BD, et al. An NR2F1-specific agonist suppresses metastasis by inducing cancer cell dormancy. *J Exp Med.* 2022;219(1):e20210836.
68. Wu R, et al. NR2F1, a tumor dormancy marker, is expressed predominantly in cancer-associated fibroblasts and is associated with suppressed breast cancer cell proliferation. *Cancers (Basel).* 2022;14(12):2962.

69. Zhang Y, et al. NR2F1-induced NR2F1-AS1 promotes esophageal squamous cell carcinoma progression via activating Hedgehog signaling pathway. *Biochem Biophys Res Commun.* 2019;519(3):497-504.
70. Liu Y, et al. Hypoxia-induced long noncoding RNA NR2F1-AS1 maintains pancreatic cancer proliferation, migration, and invasion by activating the NR2F1/AKT/mTOR axis. *Cell Death Dis.* 2022;13(3):232.
71. Castel P, et al. PDK1-SGK1 Signaling Sustains AKT-Independent mTORC1 Activation and Confers Resistance to PI3Kalpha Inhibition. *Cancer Cell.* 2016;30(2):229-42.
72. Zhang Y, et al. HSPD1 Supports Osteosarcoma Progression through Stabilizing ATP5A1 and thus Activation of AKT/mTOR Signaling. *Int J Biol Sci.* 2024;20(13):5162-90.
73. Muller J, et al. Low MITF/AXL ratio predicts early resistance to multiple targeted drugs in melanoma. *Nat Commun.* 2014;5(2014):5712.
74. Shaffer SM, et al. Rare cell variability and drug-induced reprogramming as a mode of cancer drug resistance. *Nature.* 2017;546(7658):431-5.
75. Guichard SM, et al. AZD2014, an Inhibitor of mTORC1 and mTORC2, Is Highly Effective in ER+ Breast Cancer When Administered Using Intermittent or Continuous Schedules. *Mol Cancer Ther.* 2015;14(11):2508-18.
76. Li CH, et al. Age influences on the molecular presentation of tumours. *Nat Commun.* 2022;13:208.
77. Kaur A, et al. Remodeling of the Collagen Matrix in Aging Skin Promotes Melanoma Metastasis and Affects Immune Cell Motility. *Cancer Discov.* 2019;9(1):64-81.
78. Tang Y, et al. Midkine expression by stem-like tumor cells drives persistence to mTOR inhibition and an immune-suppressive microenvironment. *Nat Commun.* 2022;13:5018.
79. Kim E, et al. Senescent fibroblasts in melanoma initiation and progression: an integrated theoretical, experimental, and clinical approach. *Cancer Res.* 2013;73(23):6874-85.

80. Elkhattouti A, et al. Stromal fibroblast in age-related cancer: role in tumorigenesis and potential as novel therapeutic target. *Front Oncol.* 2015;5:158.
81. Abel EV, and Aplin AE. FOXD3 is a mutant B-RAF-regulated inhibitor of G(1)-S progression in melanoma cells. *Cancer Res.* 2010;70(7):2891-900.
82. Teh JL, et al. An in vivo reporter to quantitatively and temporally analyze the effects of CDK4/6 inhibitor-based therapies in melanoma. *Cancer Res.* 2016;76(18):5455-66.
83. Tiago M, et al. Targeting BRD/BET proteins inhibits adaptive kinome upregulation and enhances the effects of BRAF/MEK inhibitors in melanoma. *Br J Cancer.* 2020;122(6):789-800.
84. Dobin A, et al. STAR: ultrafast universal RNA-seq aligner. *Bioinformatics.* 2013;29(1):15-21.
85. Frankish A, et al. GENCODE reference annotation for the human and mouse genomes. *Nucleic Acids Res.* 2019;47(D1):D766-D73.
86. Li B, and Dewey CN. RSEM: accurate transcript quantification from RNA-Seq data with or without a reference genome. *BMC Bioinformatics.* 2011;12:323.
87. Love MI, et al. Moderated estimation of fold change and dispersion for RNA-seq data with DESeq2. *Genome Biol.* 2014;15(12):550.
88. Subramanian A, et al. Gene set enrichment analysis: A knowledge-based approach for interpreting genome-wide expression profiles. *PNAS.* 2005;102(43):15545-50.
89. Zerbino DR, et al. The ensembl regulatory build. *Genome Biol.* 2015;16(1):56.
90. Lawrence M, et al. Software for computing and annotating genomic ranges. *PLoS Comput Biol.* 2013;9(8):e1003118.
91. Lawrence M, et al. rtracklayer: an R package for interfacing with genome browsers. *Bioinformatics.* 2009;25(14):1841-2.
92. Sandri S, et al. Vemurafenib resistance increases melanoma invasiveness and modulates the tumor microenvironment by MMP-2 upregulation. *Pharmacol Res.* 2016;111:523-33.

93. Leinonen R, et al. The sequence read archive. *Nucleic Acids Res.* 2011;39(1):D19-21.

94. Stuart T, et al. Comprehensive Integration of Single-Cell Data. *Cell.* 2019;177(7):1888-902 e21.

95. Frederick DT, et al. BRAF inhibition is associated with enhanced melanoma antigen expression and a more favorable tumor microenvironment in patients with metastatic melanoma. *Clin Cancer Res.* 2013;19(5):1225-31.